Energy 347 (2026) 140432

Contents lists available at ScienceDirect

Energy

journal homepage: www.elsevier.com/locate/energy

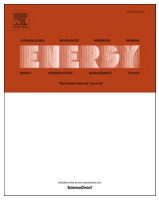

The optimal mix of flexibility in an integrated electricity-hydrogen-heating system: A case study of Great Britain in 2050

Qikun Chen *, Meysam Qadrdan

School of Engineering, Cardiff University, United Kingdom

A B S T R A C T

Flexibility is crucial in future decarbonised energy systems, compensating for the variability and uncertainty of wind and solar power generation. There already exists a significant amount of flexibility in heat and gas supply systems that can be exploited through the coordinated operation of these energy vectors with the electricity system. However, due to the complex and interdependent interactions between different energy vectors, it is challenging to quantify the amount of flexibility from the other energy vectors available to the electricity system. In this paper, we develop a modelling framework to quantify the amount of flexibility available through energy systems integration, as well as their values to the whole energy system. Using an integrated electricity, hydrogen and heat supply system for Great Britain in 2050 as a case study, the impacts of flexibility on the operational costs of the whole system, locational marginal prices of electricity, and renewable energy curtailment were investigated. The findings illustrated that unlocking whole system's flexibility can achieve over 75% operational cost savings. In addition, we examined relationship between the upward flexibility magnitude and Locational Marginal Prices of the power system and observed a negative correlation between them. This implied that busbars with greater upward flexibility are better positioned to mitigate the impacts of increasing electricity demand.

Nomenclature

1. Set (index)	Description
Gas system	
$G(g)$	All generators
$GP(gp)$	Sources of gas provision
$EL(gp)$	Networked Electrolysers ($EL \subset GP$)
$S(s)$	Gas storage sites
$P(p)$	Pipelines
$N(n)$	Nodes
$HD(hd)$	Hydrogen demand nodes ($HD \subset N$)
$C(c)$	Compressor units
$GC(c)$	Gas-driven compressor units ($GC \subset C$)
$EC(c)$	Electric-driven compressor units ($EC \subset C$)
Electricity system	
$OTH(g) \subset G$	Power generator, including nuclear, bioenergy and other renewable sources (waste, ground thermal, etc)
$GT(g) \subset G$	Gas turbines
$VRE(g) \subset G$	Renewable generators including wind farms and PV panels
$I(i)$	Interconnectors
$L(l)$	Transmission lines (wires)
$B(b)$	Busbars
$ED(ed)$	Electricity demand nodes ($ED \subset B$)
$ES(es)$	Electrical energy storage units
Heating system	
$BD(bd)$	Buildings
$HP(bd)$	Buildings installed with heat pumps ($HP \subset BD$)
$GB(bd)$	Buildings installed with gas boilers ($GB \subset BD$)
Others	
$T(t)$	Time resolution (hour)
Variables	**Description**
Gas system	
$Q^{GP}_{gp,t}$	Gas provision at t (mcm/h)
$Q^{S}_{s,t}$	Gas discharging from a storage at t (mcm/h)
$Q^{av}_{p,t}$	Average gas flow within a pipe at t (mcm/h)
$Q^{in+/out+}_{p,t}$	Positive[1] inflow/outflow of gas within a pipe at t (mcm/h)
$Q^{in-/out-}_{p,t}$	Negative inflow/outflow of gas within a pipe at t (mcm/h)
$\Pi_{n,t}$	Pressure at a gas node at t (bar)
$Q^{sup/dem}_{n,t}$	Cumulative gas supply/demand at a gas node at t (mcm/h)
$Q^{flexdem}_{n,t}$	Flexible gas demand at a gas node at t (mcm/h)
$Q^{LS}_{n,t}$	Gas load shedding at a gas node at t (mcm/h)
$Q^{tp}_{c,t}$	Gas throughput of a compressor at t (mcm/h)
$E_{c,t}$	Energy consumption of a compressor at t (MWh)
$Q^{u}_{c,t}$	Gas consumption by a compressor at t (mcm/h)
$Q^{in/out+}_{c,t}$	Positive inflow/outflow of gas within a compressor at t (mcm/h)
$Q^{in/out-}_{c,t}$	Negative inflow/outflow of gas within a compressor at t (mcm/h)
$L_{p,t}$	Volumetric value of linepack in a pipe at t (mcm)

(continued on next column)

(continued)

(continued on next page)

* Corresponding author.
E-mail address: qc0002@surrey.ac.uk (Q. Chen).

[1] In the model, the direction gas flow from n_p^{start} to n_p^{end} is considered positive, while flow from n_p^{end} to n_p^{start} is considered negative. n_p^{start} and n_p^{end} are both ends of a pipe, or suction node and discharge node of a compressor.

https://doi.org/10.1016/j.energy.2026.140432
Received 12 November 2025; Received in revised form 25 January 2026; Accepted 10 February 2026
Available online 13 February 2026

(*continued*)

$\alpha_{c,t}$	Compression ratio
$Q^{G}_{g,t}$	Gas consumed by a gas turbine at t (mcm/h)
$x_{p,t}$	Binary variables denoting the gas flow direction in a pipe at t
Electricity system	
$P^{GP}_{gp,t}$	Power consumption of an electrolyser at t (MW)
$P^{G}_{g,t}$	Power generation from a generator at t (MW)
$P^{U}_{g,t}$	Power from a renewable power station can be utilised at t (MW)
$P^{C}_{g,t}$	Curtailed renewable at a renewable power station at t (MW)
$P^{IM}_{i,t}$	Power import from an interconnector at t (MW)
$P_{l,t}$	Power flow in a wire at t (MW)
$\theta_{b,t}$	Voltage angle at a busbar at t (rad)
$P^{sup/dem}_{b,t}$	Cumulative power supply/demand at a busbar at t (MW)
$P^{flexdem}_{b,t}$	Flexible power demand at a busbar at t (MW)
$P^{LS}_{b,t}$	Power load shedding at a busbar at t (MW)
$P^{ES}_{es,t}$	Power charging/discharging of a storage unit at t (MW)
$E^{ES}_{es,t}$	Stored electrical energy in a storage unit at t (MWh)
$y_{g,t}$	Binary variable denoting the start-up process of a turbine at t, $g \subset GT$
$z_{g,t}$	Binary variable denoting the shut-down process of a turbine at t, $g \subset GT$
$u_{g,t}$	Binary variable denoting the ON/OFF process of a turbine at t, $g \subset GT$
Heating system	
$T^{in}_{bd,t}$	Indoor temperature of a building at t (K)
$P^{HP}_{bd,t}$	Power consumption of the building installed with heat pumps at t (MW)
$Q^{GB}_{bd,t}$	Gas consumption of the building installed with gas boilers at t (mcm/h)
3. Parameters	**Description**
Gas system	
$\underline{Q^{GP}_{gp}}$ / $\overline{Q^{GP}_{gp}}$	Min/max gas provision (mcm/h)
η^{EL}	Efficiency of an electrolyser
$\underline{Q^{S}_{s}}$ / $\overline{Q^{S}_{s}}$	Min/max gas discharging from an underground storage site (mcm/h)
K_p	Coefficient of gas flow of a pipe
T^{b}	Base temperature of the gas system (°R)
P^{b}	Base pressure of the gas system (psia)
Γ	Specific gravity of gas
T^{av}	Average temperature in pipelines (°R)
Z	Compressibility of gas at base temperature and pressure
Len_p	Length of a pipe (km)
D_p	Diameter of a pipe (m)
$Q^{nflexdem}_{n,t}$	Predefined non-flexible gas demand (mcm/h)
S_p	Linepack coefficient of a pipe
P	Density of gas (kg/m^3)
L^{0}_{p}	Initial linepack volume (mcm)
B, B′	Fitted coefficients of a linear expression by simplifying the nonlinear equation of compressors energy consumption
$\underline{\alpha_c}$ / $\overline{\alpha_c}$	Min/max value of compression ratio
HV	Energy content of gas (MWh/mcm)
Electricity system	
δ_g	Load factor of generator
$\underline{P^{G}_{g}}$ / $\overline{P^{G}_{g}}$	Min/max generation at generator (MW)
u^{0}_{g}	Initial ON/OFF status of gas turbine
RU_g / RD_g	Ramp-up/down rate of a gas turbine (MW/h)
SU_g / SD_g	Start-up/shut-down rate of gas turbine (MW/h)
$L^{MU/MD}$	Min-up/Min-down time of a turbine (h)
η^{G}	Efficiency of a generator
$P^{A}_{g,t}$	The available amount of renewable generation at a renewable power station (MW)
$\underline{P^{IM}_{i}}$ / $\overline{P^{IM}_{i}}$	Min/max power import from an interconnector
$\overline{P_l}$	Maximum power flow
X_l	Reactance of branch (ohm)
$P^{nflexdem}_{b,t}$	Predefined electricity demand (MW)
ES^{0}_{es}	Initial amount of energy stored in an electrical energy storage unit (MWh)
Heating system	
T^{in}_{bd,t_0}	Initial indoor temperature of a building (K)
$T^{amb}_{bd,t}$	Ambient temperature (K)
U_{bd}	Thermal conductivity (K/MW)
C_{bd}	Thermal capacity (MJ/K)

1. Introduction

The growing share of variable renewable generation technologies poses operational challenges to the power system, due to the difficulty of balancing electricity demand and supply at every moment, which is critical to maintaining the grid frequency as close as possible to its set value. The lack of sufficient flexibility[2] within the electric power system limits its ability to accommodate a high share of renewable generation technologies. For instance, an estimated 5.8 TWh of wind generation had to be curtailed in Great Britain (GB) during 2020 and 2021, which could have otherwise powered 800 thousand households [1]. The corresponding cost of the curtailed wind was £299 million in 2020 and £507 million in 2021 [1]. A flexible electric power system is able to accommodate a higher share of renewable generation, thereby reducing the curtailments and its associated costs. Recent studies indicated that with an adequate level of flexibility, the UK could yield up to £10 billion in cost savings annually by 2050 [2].

To enhance the flexibility of the GB electric power system, it is envisioned that up to 50 GW of energy storage capacity is required by 2050 [3]. While a continuous reduction of storage costs has been observed over the recent years, battery storage is still an expensive technology and there are concerns about their life cycle environmental impacts. Therefore, instead of solely relying on battery storage, through coordinated operation of multiple energy vectors, we can benefit from other flexibility sources potentials available in the different energy vectors such as heat, natural gas and hydrogen. For instance, hydrogen infrastructure can offer flexibility to the electric power system through supplying hydrogen-fired power plants [4–6] and providing large-scale within-pipe and underground storage to absorb hydrogen produced by electrolysers [5,7–9]. Hydrogen-fired power plants can help compensate for the shortfall of electricity when renewable generation is unable to meet the demand. Surplus renewable electricity can be utilised by electrolysers to produce green hydrogen, which can be stored within the hydrogen system. To ensure a resilient and efficient energy system, it is projected that Great Britain will require 30–40 GW of short-duration and 40–45 GW of long-duration flexible capacity by 2030 [10]. Several studies [11–14] demonstrated that leveraging the thermal inertia of buildings, low-carbon heating devices such as heat pumps can provide demand-side flexibility to the electric power system. Such flexibility from the heating systems in buildings enables the reduction of electricity consumption during peak demand periods while maintaining a comfortable indoor temperature for occupants. Similarly, domestic hot water tanks can act as thermal buffers that allow shifting the electricity consumption of heating water across time, thereby providing multi-gigawatt of time-shiftable thermal flexibility [15] to the power grid. For instance, Salpakari et al. [16] quantitatively evaluate how domestic hot water storage can shift electricity demand over time through optimal power-to-heat operation, thereby absorbing surplus renewable electricity and reducing peak net load in the power grid. Kirkerud et al. [17] further demonstrate that such flexibility can be aggregated and transferred across regions through district heating networks, thereby smoothing electricity price variations and enhancing renewable integration at the system level.

In addition, several emerging technologies are increasingly recognised as important providers of system flexibility. For instance, electric vehicles (EVs) can function as “mobile storage” resources, offering both upward and downward flexibility through controlled charging, vehicle-to-grid discharging, and aggregation at charging stations [18–21]. Large-scale thermal energy storage integrated into district heating

[2] In the context of electric power systems, flexibility is defined as the ability of the systems to adjust their supply and/or demand to keep them balanced at all times.

networks and electrified process heat systems can further provide substantial flexibility to the power grid. In industrial applications, electrification coupled with thermal energy storage enables temporal shifting of process heat demand, representing a major new source of flexibility [20,21]. These studies highlight flexibility opportunities across multiple layers of system integration, offering insights that support broader cross-sector coordination.

The energy systems integration has been the subject of research over the recent years. Some research has analysed the integrated energy system focusing on environmental aspects [22–25] economic perspectives [24,26,27]. However, these models are primarily designed to provide high-level insights for energy transition strategies or long-term system planning. Most of them lack a detailed representation of the energy system's operation and thus making it difficult to capture the flexibility potential of the energy system.

Some other investigations provided the operational model framework of an integrated energy system. For instance, Chen et al. [28] developed an integrated electricity-heating-hydrogen operational model to explore the role of solar generation in meeting consumers electricity demand while offering cost savings. Li et al. [29] investigated storage planning strategies in integrated energy systems using a two-stage optimisation model. However, these operational models of integrated energy systems, despite their detailed representations, mainly focus on small geographic areas, limiting their applicability to the broader or more diverse system contexts.

Several models have focused on national-scale energy systems. Franken et al. [30] developed an optimisation model of the Great Britain power system to quantify the value of demand-side flexibility from the transport and heating sectors. However, this linear model simplified the operational constraints to provide high-level insights only. Numerous studies have focused on analysing flexibility provision by specific energy vectors to electric power systems, e.g., the flexibility from linepack[3] of the gas network [31], thermal energy systems of buildings [32], and storage technologies (thermal storage [33], battery storage [34,35]). These studies demonstrate the potential and value of providing flexibility through energy systems integration. Nevertheless, accessing flexibility from an individual sector or technology fails to maximise the flexibility potential of the whole energy system.

However, exploring flexibility across the entire energy system is complex, particularly at a national scale, since the intricate interactions among different sectors. The availability of cross-vector flexibility is affected by constraints governing the operation of the energy vectors as well as the coupling components linking them. Accurately capturing the level of flexibility in different energy vectors available to electric power systems requires detailed consideration of the operational characteristics of the energy systems and the trade-offs between various sources of flexibility across the whole system.

In this paper, we explored the value of flexibility from different sources including hydrogen infrastructures, electrical energy units and residential heating system, from a whole-system perspective that accounts for their interactions. We developed an operational optimisation model of an integrated electricity-hydrogen-heating system, using the GB energy system in 2050 as a case study. The modelling framework employed in this study builds upon our previous work, such as the Combined Gas and Electricity Network (CGEN) model, which co-optimises the operation of multiple energy sectors in a synchronised manner. However, this paper extends this framework by:

- Including residential heat sector: thermal behaviour of residential buildings has been modelled using a 1R1C (also known as the single-node lumped capacitance model, is a simplified thermal model used in building energy simulations and analysis) method. Therefore, the interactions between heat demand in residential buildings and hydrogen and electricity supply system is considered in the model.
- Improving solution algorithm: the optimisation algorithm employed in this model is different from our previous study. We used Piecewise Linear (PWL) in CGEN to approximate the nonlinear formulation, however, in this work, a more efficient mathematical approach which combines McCormick Envelope and Outer Approximation is employed. This significantly improved model's performance.
- Proposing a method for quantifying flexibility from energy systems integration: This paper introduces an approach to quantify the flexibility from different energy vector available to the power system. This analysis investigated the relationship between locational flexibility and Locational Marginal Prices (LMPs) of electricity, offering new insights into spatial price signals and the system-wide value of flexibility.

In this paper, we propose a modelling framework to quantify and assess the value of flexibility in a future integrated energy system. The remainder of this paper is structured as follows. Section 2 outlines the motivation behind the study and introduces the types of flexibility sources considered. Section 3 presents the optimisation model, including the objective function, system constraints, the approach for flexibility quantification, and the method to derive Locational Marginal Prices. Section 4 describes the case study of Great Britain in 2050 and defines ten scenarios designed to explore the operational impacts of different flexibility sources. Section 5 provides the results and discussion, including the value of individual flexibility sources, quantification of system-wide flexibility, and the correlation between flexibility and electricity prices. Finally, Section 6 concludes the study and outlines directions for future research.

2. Motivation

In an integrated energy system, flexibility can be provided in different ways, as graphically described in Fig. 1. The swing in linepack helps accommodate fluctuations in supply and demand of hydrogen. Electrolysers can play a pivotal role in offering flexibility by harnessing excess energy from the electricity grid to generate hydrogen, while hydrogen-fired power plants serve as a valuable resource to supply electricity when renewable energy generation falls short of meeting electricity demand. In addition, the residential heating systems present another avenue for enhancing system flexibility. By using their thermal inertia, buildings installed with heat pumps or hydrogen boilers are capable of storing heat to manage energy consumption and maintain indoor comfort more efficiently. Moreover, electrical energy storage units like batteries and pump storage facilities offer additional flexibility to the electrical power system through their ability to charge and discharge power as needed.

Certain components, such as electrical energy storage units and electrolysers, directly contribute to the flexibility of the electric power system. Storage units could either accommodate surplus electricity or provide additional electricity through flexible charging and discharging. Electrolysers can absorb excess electrical energy. Linepack does not directly provide flexibility to the electric power system but improves the hydrogen system's capacity to handle greater fluctuations in supply and demand. This, in turn, supports the flexible operation of the coupling components like electrolysers and hydrogen-fired power plants. Likewise, heat pumps and hydrogen boilers do not independently offer demand-side flexibility; instead, they rely on the thermal inertia of building structures to regulate indoor temperatures effectively.

While these sources hold considerable potential to enhance flexibility within the whole energy system, their effectiveness is restricted by both their capacity and wider operational constraints in the system. For instance, linepack of the hydrogen transmission system is restricted by the network's pressure, preventing excessive changes in linepack. Likewise, the heating devices can only adjust their operation within a limited

[3] Linepack refers to the amount of gas that is temporarily stored within pipelines.

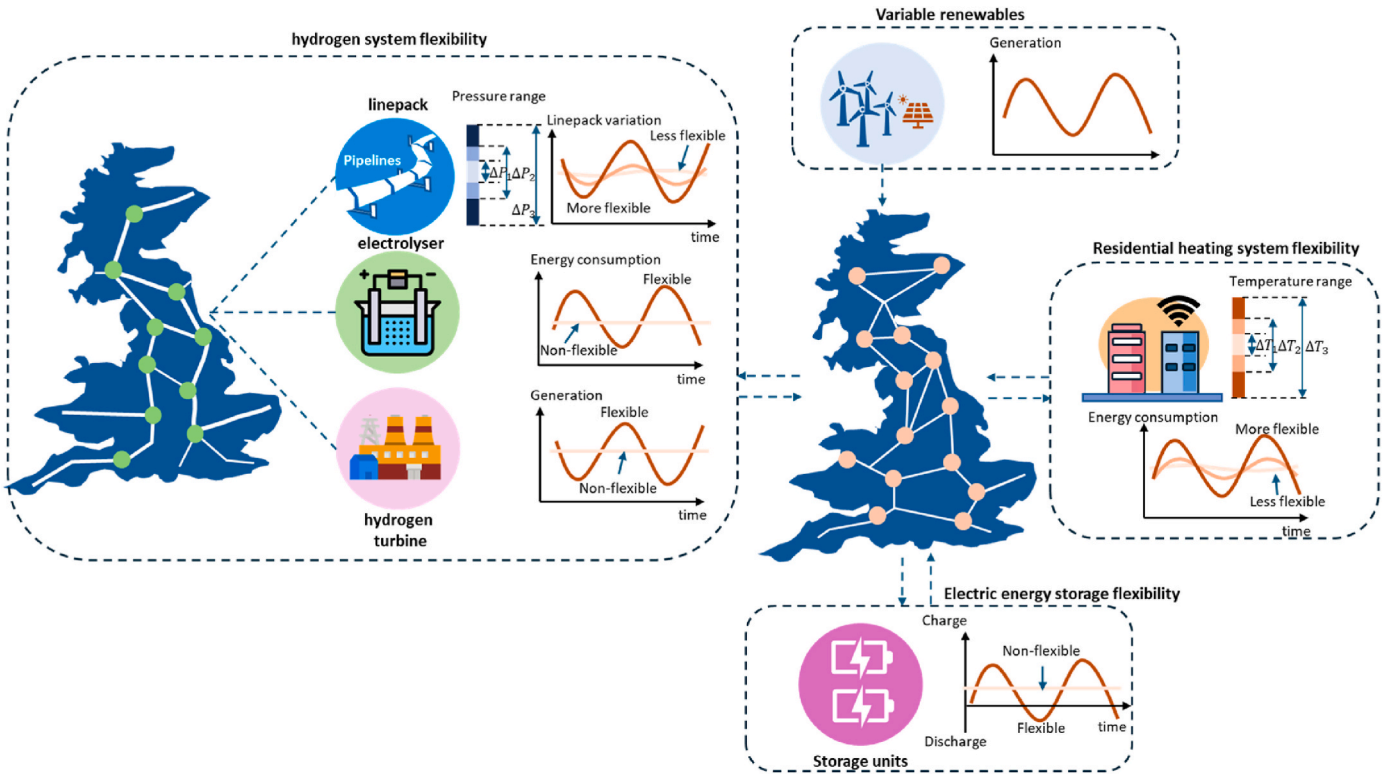

Fig. 1. Flexibility provider within the energy system.

range to maintain thermal comfort for occupants. In addition, the capacity of both electricity transmission lines and different units further limits the flexibility that can be offered by flexible resources.

Understanding the intricate interdependencies among these energy facilities within the integrated energy system is paramount for strategically managing their operations and maximising their potential to offer flexibility to the whole system. This necessitates a detailed reformulation of the whole energy system, taking into account operational characteristics of individual facilities and the physics of the networks (i.e., nodal balance).

3. Method

An optimisation model was developed to simultaneously minimise the total operating cost of integrated electricity, hydrogen and heat systems subject to physical constraints of technologies and networks. The model uses hourly timesteps and is solved over a 24-h period. The corresponding operating day is selected as a representative winter day which allows the flexibility of the residential heating system to be captured and evaluated. The applied spatial resolution is sufficient to capture geographical heterogeneity across the system, and the hourly temporal resolution accurately reflects operational dynamics; however, as noted earlier, the computational complexity of the model makes it suitable for short-term operation rather than long-term seasonal or annual optimisation.

3.1. Objective function

The objective function of the IES model is to minimise the total operational cost of integrated energy systems while adhering to the physical constraints imposed by technologies and networks, as specified in Eq. (1). Where C^{T} is the total cost of the whole system, $Q^{\mathrm{GP}}_{gp,t}$ represent amount of hydrogen produced by unit gp at time t while C^{GP} is the unit cost of hydrogen production. Similarly, $\sum_{s\in S}Q^{\mathrm{S}}_{s,t}C^{\mathrm{S}}$, $Q^{\mathrm{HLS}}_{n,t}C^{\mathrm{HLS}}$, $P^{\mathrm{G}}_{g,t}C^{\mathrm{G}}$, $\sum_{gp\in GP}P^{\mathrm{C}}_{g,t}C^{\mathrm{C}}$, $P^{\mathrm{IM}}_{i,t}C^{\mathrm{IM}}$ and $P^{\mathrm{ELS}}_{b,t}C^{\mathrm{ELS}}$ represent the hourly costs associated with hydrogen discharge from storage, hydrogen load shedding, power generation, renewable curtailment, electricity import, and electricity load shedding, respectively.

$$\begin{aligned}\mathrm{Min}\ C^{\mathrm{T}} = \sum_{t\in T}\Bigg\{&\sum_{gp\in GP}Q^{\mathrm{GP}}_{gp,t}C^{\mathrm{GP}} + \sum_{s\in S}Q^{\mathrm{S}}_{s,t}C^{\mathrm{S}} + \sum_{n\in N}Q^{\mathrm{HLS}}_{n,t}C^{\mathrm{HLS}} \\ &+ \sum_{gp\in GP}P^{\mathrm{G}}_{g,t}C^{\mathrm{G}} + \sum_{gp\in GP}P^{\mathrm{C}}_{g,t}C^{\mathrm{C}} + \sum_{i\in I}P^{\mathrm{IM}}_{i,t}C^{\mathrm{IM}} + \sum_{b\in B}P^{\mathrm{ELS}}_{b,t}C^{\mathrm{ELS}}\Bigg\}\end{aligned} \tag{1}$$

3.2. Modelling of the hydrogen network

Eq. (2) -Eq. (24) present the formulation of the hydrogen network modelling. Hydrogen provisions from different sources are denoted by Eq. (2), where GP specifies different types of hydrogen productions (including electrolysers and steamed methane reformation) while gp denotes each specific type. The networked electrolyser serves as a coupling component between the hydrogen and electricity systems. The amount of hydrogen produced by these electrolysers is determined by the amount of electricity they consume, as described in Eq. (3). The underground hydrogen storage is modelled as the backup option, offering additional provision in cases where hydrogen supply falls short of demand, albeit at a higher cost. Therefore, only the hydrogen withdrawal from the storage facility is considered. The withdrawal capacity from storage sites is represented by Eq. (4).

$$\underline{Q^{\mathrm{GP}}_{gp}} \le Q^{\mathrm{GP}}_{gp,t} \le \overline{Q^{\mathrm{GP}}_{gp}}, \forall gp \in GP, t \in T \tag{2}$$

$$\mathrm{HV}^{\mathrm{H}}Q^{\mathrm{GP}}_{gp,t} = \eta^{\mathrm{EL}}P^{\mathrm{GP}}_{gp,t}\Delta\tau, \forall gp \in EL, t \in T \tag{3}$$

$$\underline{Q^{\mathrm{S}}_{s}} \le Q^{\mathrm{S}}_{s,t} \le \overline{Q^{\mathrm{S}}_{s}}, \forall s \in S, t \in T \tag{4}$$

Since the direction of hydrogen flow within the pipe is uncertain at each time step, bi-directional flow is formulated in the model. Fig. 2

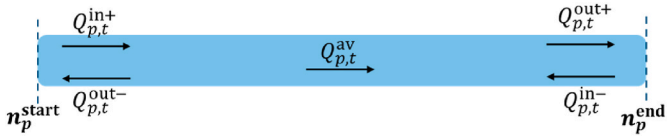

Fig. 2. Bi-directional hydrogen flow in a pipe.

$$Q^{av}_{p,t} = 0.5\left(Q^{in+}_{p,t} + Q^{out+}_{p,t}\right) - 0.5\left(Q^{in-}_{p,t} + Q^{out-}_{p,t}\right), \forall p \in P, t \in T \quad (5)$$

presents the bi-directional hydrogen in a pipe. Note that, n_p^{start}, n_p^{end} are two ends of a pipe, it is assumed that, the direction hydrogen flow from n_p^{start} to n_p^{end} is considered positive, while flow from n_p^{end} to n_p^{start} is considered negative. Where $Q^{in/out+}_{p,t}$ denote the positive inflow/outflow of hydrogen while $Q^{in/out-}_{p,t}$ represent the negative inflow/outflow rate of hydrogen through a pipe p. $Q^{av}_{p,t}$ is the average hydrogen flow rate in pipe p, and can be calculated by Eq. (5)

The hydraulic flow equation which is used to clarify the relationship between flow rate and pressure drop within a pipe, is considered and denoted by Eq. (6). Where $\Pi_{n_p^{start}}$ and $\Pi_{n_p^{end}}$ are pressure value at node both ends of a pipe, respectively. K_p is the flow coefficient calculated by Eq. (7) [36].

$$Q^{av}_{p,t}\left|Q^{av}_{p,t}\right| = K_p^2\left(\Pi^2_{n_p^{start},t} - \Pi^2_{n_p^{end},t}\right), \forall p \in P, \forall t \in T \quad (6)$$

$$K_p = \sqrt{\frac{33 D_p^{53}\left(\frac{T^b}{P^b}\right)^{1.02}}{T^{av} \times Z \times Len_p \times \gamma^{0.961}}}, \forall p \in P, t \in T \quad (7)$$

Within the hydrogen network, the mass conservation (also referred to as nodal balance) is taken into account. Eq. (8) is the nodal balance equation for the pipeline network, ensuring that the hydrogen inflow at each node n is equal to the hydrogen outflow from that same node at all timesteps. Fig. 3 graphically illustrates an example of nodal balance. Where $Q^{sup}_{n,t}$ represents the cumulative hydrogen provision at node n at time t, sourced from hydrogen terminals, electrolysers, and hydrogen storage facilities. The hydrogen demand $Q^{dem}_{n,t}$ represents the comprehensive hydrogen demand at the same node.

The cumulative hydrogen demand at each node, represented by

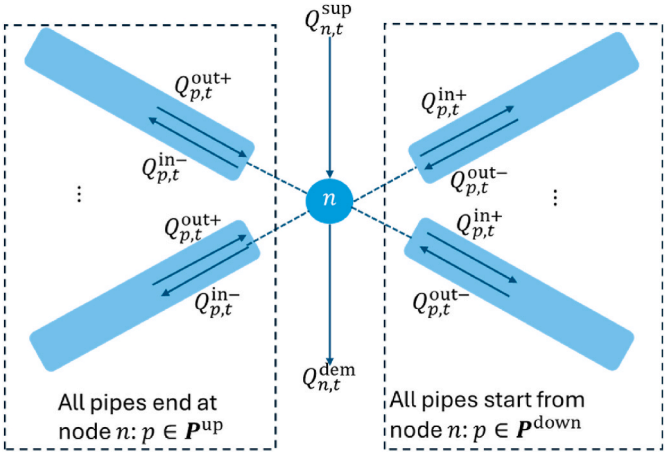

Fig. 3. Diagram of nodal balance in the hydrogen network.

$$Q^{sup}_{n,t} - Q^{dem}_{n,t} + \sum_{p \in P^{up}}\left(Q^{out+}_{p,t} - Q^{in+}_{p,t}\right) + \sum_{p \in P^{down}}\left(Q^{out-}_{p,t} - Q^{in-}_{p,t}\right) = 0, \forall n \in N, t \in T \quad (8)$$

$Q^{dem}_{n,t}$, is divided into two distinct categories: 'flexible' and 'non-flexible' demands, as outlined in Eq. (9). The flexible demand includes the hydrogen demand for power generation, heating, hydrogen-driven compressors, which is determined endogenously in the model to achieve a cost-optimal operation strategy. The remaining energy demands are assumed to be non-flexible[4] and predetermined and are inputs to the model. Where $Q^{flexdem}_{n,t}$ denotes flexible demand while $Q^{nflexdem}_{n,t}$ represents the 'non-flexible' demand. Load shedding is considered, to prevent the system from overloading, as denoted by Eq. (10). $Q^{HLS}_{n,t}$ represents the rate of hydrogen load shedding. A high penalty cost for hydrogen load shedding is considered, to ensure its minimisation by the optimisation model, as illustrated in objective function.

$$Q^{dem}_{n,t} = Q^{flexdem}_{n,t} + Q^{nflexdem}_{n,t}, \forall n \in N, t \in T \quad (9)$$

$$Q^{HLS}_{n,t} \le Q^{nflexdem}_{n,t}, \forall n \in N, t \in T \quad (10)$$

Within the pipeline system, the linepack which refers the amount of hydrogen that can be temporarily stored within the pipeline, and is formulated by Eq. (11) - Eq. (15). Eq. (11) describes the relationship between linepack in pipeline p and pressure at both ends of the pipe. $L_{p,t}$ is the linepack volume of pipeline p at time t and S_p is the linepack coefficient determined by Eq. (12). Eq. (13) and Eq. (14) establish the continuity of linepack across time steps t (current timestep) and previous timestep. $L_{p,t}$ is the volumetric value of linepack in a pipe p, L^0_p represents the predefined initial linepack indicating the original linepack volume before optimisation. Eq. (15) indicates the linepack at the end of day should be equal or greater than initial volume, ensuring the level of it is enough for the next day. This equation can be modified to impose any other target for the end-of-day linepack.

$$L_{p,t} = S_p \frac{\Pi_{n_p^{start},t} + \Pi_{n_p^{end},t}}{2}, \forall p \in P, t \in T \quad (11)$$

$$S_p = \frac{\pi \times Len_p \times D_p^2}{4 \times Z \times T^b \times \rho}, \forall p \in P, t \in T \quad (12)$$

$$L_{p,t_1} = L^0_p + Q^{in+}_{p,t_1} - Q^{out+}_{p,t_1} + Q^{in-}_{p,t_1} - Q^{out-}_{p,t_1}, \forall p \in P, t = t_1 \quad (13)$$

$$L_{p,t} = L_{p,t-1} + Q^{in+}_{p,t} - Q^{out+}_{p,t} + Q^{in-}_{p,t} - Q^{out-}_{p,t}, \forall p \in P, t \ne t_1 \quad (14)$$

$$L_{p,t24} \ge L^0_p, \forall p \in P \quad (15)$$

To ensure sufficient flow, compressor units which are installed along pipelines are considered in the modelling of transmission system. These units are capable of boosting pressure, addressing the critical need for ensuring a safe operation. Two types of compressor units are considered: Electric-driven Compressor (EDC) and Hydrogen-driven Compressor (GDC). The energy consumption of each compressor can be expressed by Eq. (16). Where $E_{c,t}$ is the energy consumption of a compressor unit c, B and B′ are fitted coefficients to linearise the original nonlinear formulation, $Q^{tp}_{c,t}$ is the hydrogen throughput and $\alpha_{c,t}$ is the compression ratio, which is restricted by Eq. (17). Eq. (18) and Eq. (19) are employed so that negative flow (flow from discharge node to suction node) is not allowed within a compressor. The pressure increases after being boosted by the compressor is denoted by Eq. (20). Where n_c^{end} is the discharge node of a compressor c while n_c^{start} is the suction node of it. The amount of hydrogen throughput should be equivalent to that of hydrogen positive

[4] The annual demand data used in this study are taken from the Future Energy Scenario (FES) 2050 projections [40]. For hydrogen, the heating-related portion is removed and the remaining demand is treated as non-flexible, which is then converted into a daily average. The same approach is applied to the electricity demand.

outflow, expressed as Eq. (21).

$$E_{c,t} = \mathrm{B}Q^{\mathrm{tp}}_{c,t} + \mathrm{B}'\alpha_{c,t}, \forall\, c \in C, t \in T \tag{16}$$

$$\underline{\alpha_c} \le \alpha_{c,t} \le \overline{\alpha_c}, \forall\, c \in C, t \in T \tag{17}$$

$$Q^{\mathrm{in}-}_{c,t} = 0, \forall\, c \in C, t \in T \tag{18}$$

$$Q^{\mathrm{out}-}_{c,t} = 0, \forall\, c \in C, t \in T \tag{19}$$

$$\Pi_{n^{\mathrm{end}}_c,t} = \Pi_{n^{\mathrm{start}}_c,t}\alpha_{c,t}, \forall\, c \in C, t \in T \tag{20}$$

$$Q^{\mathrm{tp}}_{c,t} = Q^{\mathrm{out}+}_{c,t}, \forall\, c \in C, t \in T \tag{21}$$

Mass conservation of hydrogen through a compressor unit is maintained, as denoted by Eq. (22). If the compressor runs on hydrogen, the amount of hydrogen consumed by the compressor can be calculated by Eq. (23). If the compressor is driven by electricity, $Q^{\mathrm{u}}_{c,t} = 0$ and the hydrogen inflow of the compressor equals to hydrogen outflow of this compressor, as denoted by denoted by Eq. (24).

$$Q^{\mathrm{out}+}_{c,t} + Q^{\mathrm{u}}_{c,t} = Q^{\mathrm{in}+}_{c,t}, \forall\, c \in C, t \in T \tag{22}$$

$$Q^{\mathrm{u}}_{c,t} = \frac{E_{c,t}}{\mathrm{HV}}, \forall\, c \in GC, t \in T \tag{23}$$

$$Q^{\mathrm{in}+}_{c,t} = Q^{\mathrm{out}+}_{c,t}, \forall\, c \in EC, t \in T \tag{24}$$

3.3. Modelling of the electricity network

In the modelling of the electricity system, different types of power generator, transmission wires and electric energy storage units are considered. Within the electricity system, the power generation from different types of power stations is modelled by Eq. (25) and Eq. (26). Eq. (25) denotes the power generation including nuclear, bioenergy and other renewable sources (e.g., ground thermal energy, waste, etc), which is fixed over optimisation timesteps. Where $P^{\mathrm{G}}_{g,t}$ is the power generation, $\overline{P^{\mathrm{G}}_g}$ is the capacity of the power station g and δ_g is the capacity factor. Eq. (26) represents the power generation from hydrogen turbines, considering its operational status. Where $u_{g,t}$ is a set of binary variables, denoting ON/OFF status of hydrogen turbine g. For instance, when $u_{g,t} = 1$, the turbine is working within the operational bounds [$\underline{P^{\mathrm{G}}_g}$, $\overline{P^{\mathrm{G}}_g}$], and when $u_{g,t} = 0$, it is offline and $P^{\mathrm{G}}_{g,t} = 0$.

$$P^{\mathrm{G}}_{g,t} = \delta_g \overline{\mathrm{P}^{\mathrm{G}}_g}, \forall g \in OTH, t \in T \tag{25}$$

$$u_{g,t}\underline{\mathrm{P}^{\mathrm{G}}_g} \le P^{\mathrm{G}}_{g,t} \le u_{g,t}\overline{\mathrm{P}^{\mathrm{G}}_g}, \forall g \in GT, t \in T \tag{26}$$

The detailed representation of the operational status of hydrogen turbines are given by Eq. (27) – Eq. (29). These constraints are employed to ensure that the turbine cannot be in both start-up and shut-down state at the same time. Where $y_{g,t}$ and $z_{g,t}$ are sets of binary variables associated with turbine's start-up and shut-down processes, respectively. If $y_{g,t} = 1$, the turbine g is starting up; if $z_{g,t} = 1$, it is shutting down. It is not possible for the turbine to be in both start-up and shut-down states simultaneously, as constrained by Eq. (27). $u_{g,t}$ is a set of binary variables denoting the ON/OFF status of a turbine and u^0_g is the initial ON/OFF status of it. Eq. (28) delineates the relationship between the start-up process, shut-down process and ON/OFF status of a turbine at the first time step t_1, while Eq. (29) details this relationship for all other timesteps.

$$y_{g,t} + z_{g,t} \le 1, \forall g \in GT, t \in T \tag{27}$$

$$y_{g,t_1} - z_{g,t_1} = u_{g,t_1} - u^0_g, \forall g \in GT, t = t_1 \tag{28}$$

$$y_{g,t} - z_{g,t} = u_{g,t} - u_{g,t-1}, \forall g \in GT, t \in T \backslash t_1 \tag{29}$$

Eq. (30) and Eq. (31) constrain the ramp-up rate and ramp-down rate of turbine within an allowable range, respectively. Where RU_g is ramp-up rate, SU_g is the start-up rate, RD_g is ramp-down rate and SD_g is shut-down rate. Eq. (32) to Eq. (35) specify the minimum up time and minimum down time constraints for the turbine. In the operation of turbine, minimum up time is the minimum period that a turbine must be kept running once it has been started up while minimum up time refers to the minimum period that a power plant must remain offline once it has been turned off. Where L^{MU} is the minimum up time and L^{MD} is the minimum down time.

$$P^{\mathrm{G}}_{g,t} - P^{\mathrm{G}}_{g,t-1} \le \mathrm{RU}_g\left(1 - y_{g,t}\right) + \mathrm{SU}_g y_{g,t}, \forall g \in GT, t \in T \tag{30}$$

$$P^{\mathrm{G}}_{g,t-1} - P^{G}_{g,t} \le \mathrm{RD}_g\left(1 - z_{g,t}\right) + \mathrm{SD}_g z_{g,t}, \forall g \in GT, t \in T \tag{31}$$

$$\sum_{t=t_k}^{t=t_{k+(\mathrm{L}^{\mathrm{MU}}-1)}} u_{g,t} \ge \mathrm{L}^{\mathrm{MU}} \times y_{g,t_k}, 1 \le k \le 21, \forall g \in GT, t \in T \tag{32}$$

$$\sum_{t=t_k}^{t=t_{24}} \left(u_{g,t} - y_{g,t_k}\right) \ge 0, 22 \le k \le 24, \forall g \in GT, t \in T \tag{33}$$

$$\sum_{t=t_k}^{t=t_{k+(\mathrm{L}^{\mathrm{MD}}-1)}} \left(1 - u_{g,t}\right) \ge \mathrm{L}^{\mathrm{MD}} \times z_{g,t_k}, 1 \le k \le 21, \forall g \in GT, t \in T \tag{34}$$

$$\sum_{t=t_k}^{t=t_{24}} \left(1 - u_{g,t} - z_{g,t_k}\right) \ge 0, 22 \le k \le 24, \forall g \in GT, t \in T \tag{35}$$

The hydrogen turbine serves as a linkage between the hydrogen system and the electricity system, since the amount of electricity it can generate is determined by its hydrogen consumption, as specified in Eq. (36). Eq. (37) is the constraint governing power generation from VRE sources, encompassing both wind generation and solar generation. Where $P^{\mathrm{U}}_{g,t}$ is the amount of power injected into the grid from the power station g, $P^{\mathrm{C}}_{g,t}$ is the curtailed renewable generation and $\mathrm{P}^{\mathrm{A}}_{g,t}$ specifies the available amount of renewable generation at this power station, which is predetermined as input data. Furthermore, Equation (38) serves as the constraint governing electricity import via interconnectors. In this case study, we simplify the analysis by not delving into the intricate energy markets for import and export. Instead, we assign a relatively high value to the import cost. This ensures that electricity is imported only when domestic supply falls short of meeting demand.

$$P^{\mathrm{G}}_{g,t}\Delta\tau = \eta^{\mathrm{G}}\mathrm{HV}^{\mathrm{G}}Q^{\mathrm{G}}_{g,t}, \forall g \in GT, t \in T \tag{36}$$

$$P^{\mathrm{U}}_{g,t} + P^{\mathrm{C}}_{g,t} = \mathrm{P}^{\mathrm{A}}_{g,t}, \forall g \in VRE, t \in T \tag{37}$$

$$\underline{P^{\mathrm{IM}}_i} \le P^{\mathrm{IM}}_{i,t} \le \overline{P^{\mathrm{IM}}_i}, \forall i \in I, t \in T \tag{38}$$

The DC power flow is formulated in the modelling of the electricity transmission network. The DC flow is simplified from the AC power flow based on the following assumptions:

1. In high-voltage transmission systems, line resistance is much smaller than line reactance, so resistance and system losses can be ignored.
2. The phase voltage angle difference in a high-voltage line is very small.
3. The bus voltage per unit is close to the nominal value.

A linear power flow equation is employed to in the model, as denoted by Eq. (39) and Eq. (40). Where $P_{l,t}$ is the power flow at wire l while $\overline{P}_l$ is the transmission capacity of l, $\theta_{b^{\mathrm{start}}_l,t}$ and $\theta_{b^{\mathrm{end}}_l,t}$ are the voltage angles at

the start and end of this wire, respectively, and X_l is the reactance of the wire l

$$-\overline{P}_l \le P_{l,t} \le \overline{P}_l, \forall l \in L, \forall t \in T \tag{39}$$

$$P_{l,t} = \left(\theta_{b_l^{\text{start}},t} - \theta_{b_l^{\text{end}},t}\right) \Big/ X_l, \forall l \in L, \forall t \in T \tag{40}$$

The nodal balance (energy conservation) is considered, as denoted by Eq. (41). This constraint ensures that the inflow of power at each busbar b must be equal to the power outflow from that same busbar. Fig. 4 presents a simple example of the nodal balance within the electric power system. Where $P_{b,t}^{\text{sup}}$ denotes the total amount of power injected into the busbar b, from all generators and discharged power from the batter/pump storage that connected with b. $P_{b,t}^{\text{dem}}$ represents the total amount of power demand from this node.

Similar to the modelling of the hydrogen system, flexible and non-flexible power demands are incorporated in the electricity model, as denoted by Eq. (42). Where $P_{b,t}^{\text{flexdem}}$ denotes flexible power demand, which includes demand for heating, electrolysers and electric-driven compressor units. It is optimised endogenously by the model. $P_{b,t}^{\text{nflexdem}}$ represents the remaining power demand classified as 'non-flexible' power demand, which is pre-determined as input data. Load shedding is considered, to prevent the electricity system from overloading, as denoted by Eq. (43).

$$P_{b,t}^{\text{dem}} = P_{b,t}^{\text{flexdem}} + P_{b,t}^{\text{nflexdem}}, \forall b \in B, t \in T \tag{42}$$

$$P_{b,t}^{\text{LS}} \le P_{b,t}^{\text{nflexdem}}, \forall b \in B, t \in T \tag{43}$$

Eq. (44)- Eq. (46) represent the operation of the electricity storage units (including battery storage and pumped storage). Eq. (44)- Eq. (45) establish the continuity of energy storage across adjacent timesteps. Where $ES_{es,t}$ is the amount of energy stored in units es, $P_{es,t_1}^{\text{ES}}\Delta\tau$ denotes the amount of electrical energy being charged (when $P_{es,t}^{\text{ES}} \ge 0$) or discharged (when $P_{es,t}^{\text{ES}} \le 0$). ES_{es,t_0} represents the predefined initial level of energy stored in the unit es. ES_{es}^0 is the initial amount of energy stored in the unit es. Eq. (46) signifies that the energy storage of the unit es at the end of the day must be equal to or greater than its initial value, ensuring that the stored energy level is sufficient for the next day's requirements.

$$E_{es,t_1}^{\text{ES}} = \text{ES}_{es}^0 + P_{es,t_1}^{\text{ES}}\Delta\tau, \forall es \in ES, t = t_1 \tag{44}$$

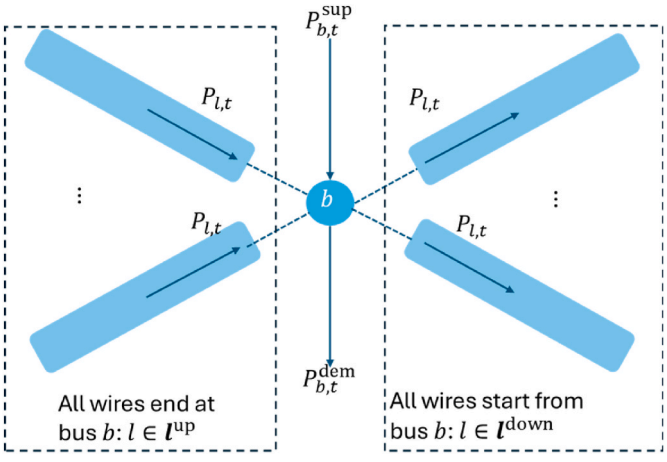

Fig. 4. Diagram of nodal balance in the electric power system.

$$P_{b,t}^{\text{sup}} - P_{b,t}^{\text{dem}} + \sum_{l \in l^{\text{up}}} P_{l,t} - \sum_{l \in l^{\text{down}}} P_{l,t} = 0, \forall b \in B, t \in T \tag{41}$$

$$E_{es,t}^{\text{ES}} = ES_{es,t-1}^{\text{ES}} + P_{es,t}^{\text{ES}}\Delta\tau, \forall es \in ES, t \ne t_1 \tag{45}$$

$$ES_{es,t_{24}}^{\text{ES}} \ge \text{ES}_{es}^0, \forall es \in ES \tag{46}$$

3.4. Modelling of the residential heating network

Within the IES model, the energy consumption of residential heating is considered. Multiple buildings in different locations are simplified to a single building, where they share the same averaged value for thermal characteristics of building materials, such as thermal capacity and thermal conductivity.

Thermal balance [37] of the building is considered and outlined as Eq. (47) and Eq. (48). Eq. (47) establishes the relationship between indoor temperature at $t_0 = 21°C$ (initial timestep before optimisation) and t_1, ambient temperature ($T_{b,t}^{\text{amb}}$) and heat load $H_{b,t}$ in buildings at busbar b. Where U_b is the averaged value of thermal conductivity of buildings at b and C_b is the averaged value of thermal capacity of these buildings. Eq. (48) applies similar considerations for other time steps beyond t_1. T_{bd,t_1}^{amb} is the ambient temperature as predefined as input data, while the indoor temperature is variable which can be affected by ambient temperature and heat supply $H_{bd,t}$.

$$\begin{aligned} T_{bd,t_1}^{\text{in}} &= e^{-\frac{3600U_{bd}}{C_{bd}}} T_{bd,t_0}^{\text{in}} + \left(1 - e^{-\frac{3600U_{bd}}{C_{bd}}}\right) T_{bd,t_1}^{\text{amb}} \\ &+ \frac{1}{U_{bd}} \left(1 - e^{-\frac{3600U_{bd}}{C_{bd}}}\right) H_{bd,t}, \forall bd \in BD, t = t_1 \end{aligned} \tag{47}$$

$$\begin{aligned} T_{bd,t}^{\text{in}} &= e^{-\frac{3600U_{bd}}{C_{bd}}} T_{bd,t-1}^{\text{in}} + \left(1 - e^{-\frac{3600U_{bd}}{C_{bd}}}\right) T_{bd,t}^{\text{amb}} \\ &+ \frac{1}{U_{bd}} \left(1 - e^{-\frac{3600U_{bd}}{C_{bd}}}\right) H_{bd,t}, \forall bd \in BD, t \ne t_1 \end{aligned} \tag{48}$$

The required energy for residential buildings equipped with air source heat pumps (expressed by $\forall b \in HP$) to satisfy the heat demand is calculated by Eq. (49). Where $\text{COP}_{bd,t}$ is the coefficient of performance impacted by the ambient temperature and can be calculated by Eq. (50).

$$H_{bd,t}^{\text{HP}} = \text{COP}_{bd,t} P_{bd,t}^{\text{HP}} \Delta\tau, \forall bd \in HP, t \in T \tag{49}$$

$$\text{COP}_{bd,t} = 3 + \left(T_{bd,t}^{\text{amb}} - 270.5\right) \Big/ 15, \forall bd \in HP, t \in T \tag{50}$$

The indoor temperature of all buildings is constrained within 18–24 °C on an hourly basis, and the 24-h average indoor temperature is fixed at 21 °C, such that the solution can exploit operational flexibility without staying at the lower indoor temperature bound purely to minimise cost. Additionally, since the optimisation timestep is 1 h, and the measured ramping behaviour of residential heat pumps occurs within minutes [38], explicit ramp-rate constraints are not required.

3.5. An approach to quantify flexibility magnitude

Fig. 5 illustrates the structure of the integrated energy system optimisation model and an approach to quantify the flexibility of the system. Fig. 5a presents the overview of the integrated energy system modelling framework. An input database includes capacity of different technologies, demand profile, temperature profile, number of dwellings and geographic information (i.e., network topology, location of residential buildings), as well as the cost assumptions and data. Within the IES model, we take account of the detailed constraints such as: physical characteristics for both hydrogen transmission and electricity

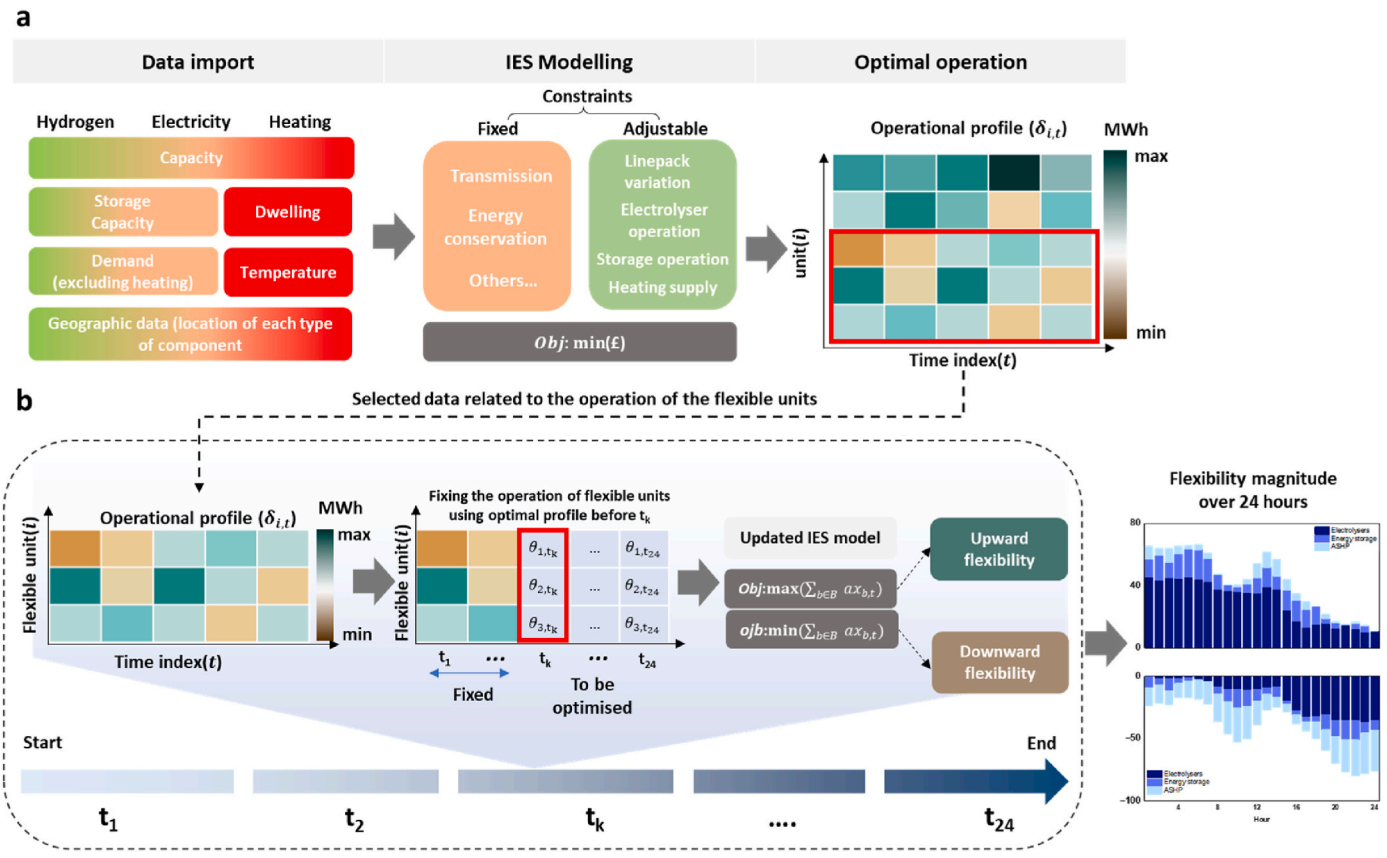

Fig. 5. The structure of the optimisation model for IES. a, Modelling framework of the IES. **b,** post-analysis approach for quantifying flexibility of the system. Note that in the context of generation technology, the ability to increase output is referred to as upward flexibility, while the ability to decrease output is called downward flexibility. On the demand side, the terms are reversed.

$$P_{b,t}^{\sup} - P_{b,t}^{\text{dem}} + \sum_{l\in L_b^{\text{up}}} P_{l,t} - \sum_{l\in L_b^{\text{down}}} P_{l,t} = ax_{b,t}, \forall b \in B, t \in T \tag{51}$$

transmission (i.e., hydraulic hydrogen flow and power flow equations), energy conservation and thermal state formulation for the residential heating system. These formulations ensure that the model produces operationally feasible and realistic outputs.

The results derived from the least-cost optimisation are used as an input database for quantifying flexibility, and Fig. 5b provides an example on how flexibility is quantified. In this phase, the primary focus is not on operational cost, instead, the objective is to determine the maximum flexibility different units can provide. We formulate the original nodal balance equation from Eq. (41) to Eq. (51), by introducing a set of auxiliary variables $ax_{b,t}$.

To quantify the magnitude of flexibility available from each source, initially, the optimal solution matrix δ_{it}, which incorporates the operational data of all flexible units (electricity consumption of heat pumps and electrolysers, charging and discharging of electrical energy storage units), needs to be imported into the updated IES model for flexibility quantification. Note that, the main focus of this paper is alternative sources of flexibility therefore we did not consider the flexibility from power stations. To quantify flexibility at t_k, the decision variables $\theta_{i,t}$ representing the operation of each flexible unit should be fixed to the corresponding values in $\delta_{i,t}$ for all timesteps before t_k (i.e., $\theta_{i,t} = \delta_{i,t}, t < t_k$). Then maximising $\sum_{b\in B} ax_{b,t}$ and upward flexibility can be calculated by $\sum_{i\in I}\left(\theta_{i,t_k} - \delta_{i,t_k}\right)$. The downward flexibility can be quantified using the same approach but minimising the $\sum_{b\in B} ax_{b,t}$. Note that when quantifying flexibility at each timestep, decision variables such as electricity imports, hydrogen and electricity load shedding, and renewable curtailment have to be fixed. This ensures that the analysis exclusively measures the inherent flexibility of the system.

3.6. LMP calculations

To capture the value of LMP at each Busbar, it is required to get the dual value of the energy balance constraints. A simple example is given below to present the way to calculate the LMP of each Busbar. Eq. (52) is the Lagrangian formulation (LA_b) of the of original problem, where $P_{b,t}^{\text{in}} - P_{b,t}^{\text{out}} + \sum_{l\in L_b^{\text{up}}} P_{l,t} - \sum_{l\in L_b^{\text{down}}} P_{l,t}$ is the nodal balance, $f(x_b)$ denotes other constraints at b. Then the LMP value λ_b can be calculated by Eq. (53).

$$LA_b = C + \lambda_b\left(P_b^{\sup} - P_b^{\text{dem}} + \sum_{l\in L^{\text{up}}} P_{l,t} - \sum_{l\in L^{\text{down}}} P_{l,t}\right) + \mu f(x_b) \tag{52}$$

$$\lambda_b = \frac{\partial LA_b}{\partial P_b^{\text{dem}}} \tag{53}$$

Note that LMP values are not explicitly defined as decision variables in the optimisation model. After the Mixed-Integer Problem (MIP) is solved and the optimal solution is obtained, the binary variables from

this solution are fixed at their optimal integer values, and the model effectively reduces to a linear problem (LP). The LMP values reported in this paper are then obtained in a post-processing step and calculated as the dual values of the nodal power balance constraints of the resulting LP, as provided by the Gurobi solver.

4. Case study and scenarios

We used Great Britain (GB) in the year 2050 as a case study to investigate the value of flexibility and the optimal mix of flexibility in an integrated electricity, hydrogen and heat system. This study assumes the existence of a national hydrogen network by 2050. This assumption is consistent with the "Project Union" initiative by National Gas, which proposes repurposing parts of the 5000-mile National Transmission System (NTS) to transport 100% hydrogen [39]. Moreover, the System Transformation scenario in the FES [40] published by the National Energy System Operator (NESO) envisages the highest hydrogen demand among all decarbonisation pathways, further supporting the plausibility of a national-scale hydrogen infrastructure. While forward-looking, this assumption aligns with existing policy directions and provides a useful basis for exploring long-term system integration and flexibility. This section details the relevant case assumptions, data sources and simulation scenarios adopted in the modelling framework.

4.1. An integrated electricity-hydrogen-heating system in GB 2050

As illustrated in Fig. 6a, the electricity and hydrogen infrastructure networks are linked through hydrogen-fired power plants, networked electrolysers, and electric-driven hydrogen compressors (EDCs). Furthermore, the residential heat sector, i.e. heat demand and heating technologies in residential buildings, is connected to the electricity and hydrogen networks through heat pumps and hydrogen boilers, respectively.

Fig. 6b shows the intricate interactions between each facility within the integrated energy system. Within the electricity system, we consider diverse generation types including wind, solar, nuclear, biomass, and hydrogen-fired generation. Electricity from these sources is transmitted across the grid via transmission lines. Electrical energy storage units such as batteries and hydro pumps are integrated into the power grid, to help balance supply and demand timely. In the hydrogen system, hydrogen is produced either through Steam-Methane Reformation (SMR) technology or electrolysis, and delivered to different offtake points via pipelines. Although underground hydrogen storage is included, the model, focusing on short-term operations, does not account for the flexible charging and discharging of hydrogen storage. Instead, hydrogen storage serves as a backup to address shortfalls in hydrogen supply.

The demand for hydrogen and electricity is categorised into two distinct types 'flexible' and 'nonflexible' demands. In this study, the flexible demand includes electricity and hydrogen demand for heating in residential buildings, electricity demand for electrolysers, electricity demand for electric-driven compressors, and hydrogen demand for hydrogen-fired power plants. The flexible demands are determined endogenously in the model to achieve a cost-optimal operation strategy, subject to meeting the demand for energy services (e.g., maintaining the indoor temperature of the residential building within a comfortable range). The remaining energy demands are assumed to be nonflexible and predetermined and are inputs to the model.

Table 1 shows the capacities of technologies, interconnectors and storage units in 2050. These assumptions are based on the 'System Transformation Scenario' proposed by FES [3]. In the System Transformation Scenario, it is assumed that hydrogen will have widespread uses across different sectors including industry, heating and transport. The share of wind and solar in the electricity generation mix will be approximately 68%.

Additionally, the operational cost of each component within the integrated energy system is outlined in Table 2. Note that, some assumptions have been made in the model. For example, the model used a

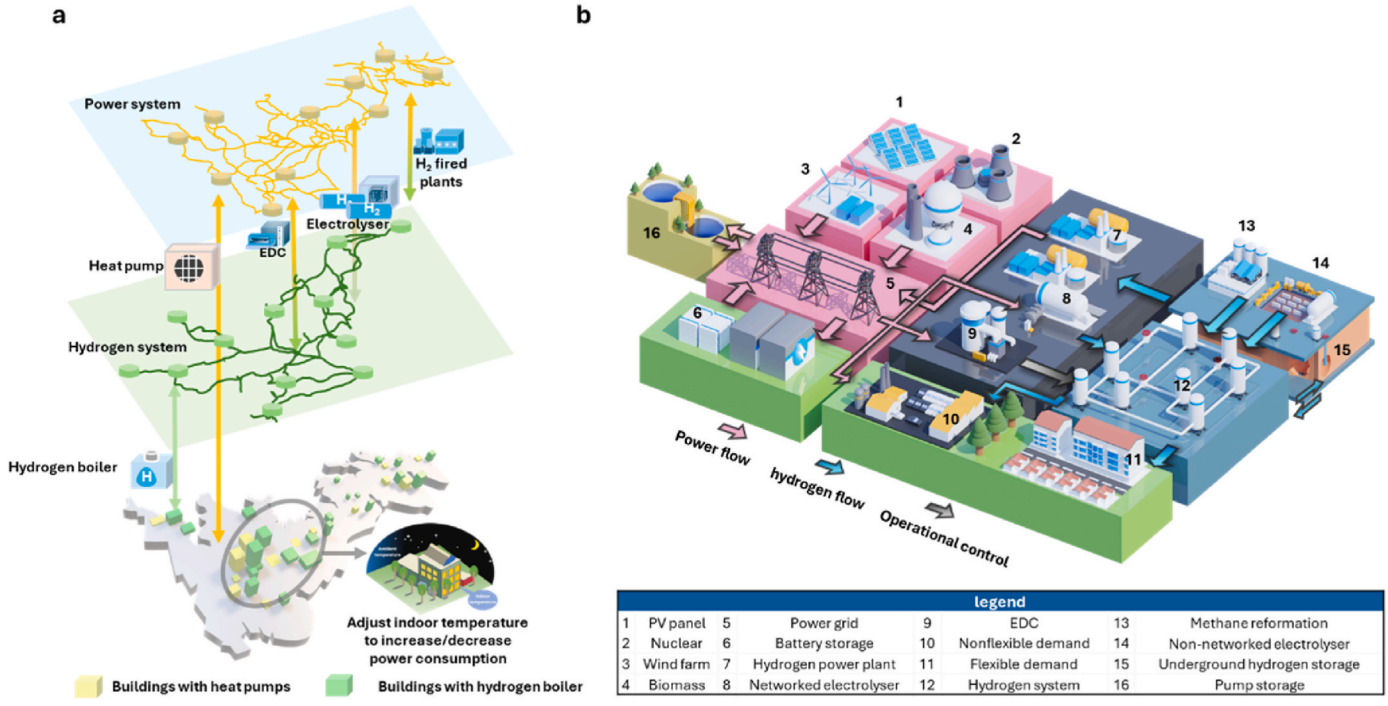

Fig. 6. Overview of the integrated energy systems. **a**, the links between the electricity system, hydrogen system and residential heat sector, through hydrogen-fired power plants, electrolysers, electric-driven compressors and buildings installed with hydrogen boilers and heat pumps. **b**, interactions across facilities within the integrated energy systems. The figure illustrates the supply and demand side and the sources of flexibility. Note that, the generation from nuclear and bioenergy is predefined as parameter. Additionally, the available generation from wind and PV sources is predefined as input data, but the amount of power that can be integrated into the electric power system and the level of renewable curtailment required are variables that will be determined by the optimisation model.

Table 1
Capacity of technologies in 2050. We established a simplified GB electricity network with 30 Busbars, based on Electricity Ten Year Statement (ETYS) [41] map. The detailed network map of both the electric power grid and hydrogen network can be found in the appendix. Since the lack of details, the capacity of heating technologies in the future is assumed using the approach proposed by Ref. [42]. Both onshore and offshore wind profiles are derived from the Renewable Ninja dataset, using geospatially resolved wind speed data for offshore locations. Although onshore and offshore generation potentials are incorporated as inputs, the actual dispatch and curtailment are determined endogenously by the optimisation model, subject to network constraints such as transmission capacity and nodal balance.

Sectors	Technologies	Capacity (GW)
Hydrogen production	Blue hydrogen production (Methane reformation with CCUS)	26
	Green hydrogen (via networked electrolysers)	38
	Green hydrogen (via non-networked electrolysers)	15
Electricity generation	Hydrogen-fired power plant	22
	Onshore wind	34
	Offshore wind	97
	PV	57
	Nuclear	13
	Bioenergy	11
	Other renewable (made up of waste, hydro, marine)	13
	Interconnector	16
Heating supply	Air Source Heat Pump (ASHP)	34
	Hydrogen boiler	67

Table 2
Cost of each component within the integrated energy system.

Sector	Components	Cost	Unit
Electricity	Nuclear	10	GBP/MWh
	Biomass	44	GBP/MWh
	Start-up of hydrogen turbine	418-92021 (determined by the capacity of the turbine)	GBP
	Renewable curtailment	40	GBP/MWh
	Import	500	GBP/MWh
	Electricity load shedding	50000	GBP/MWh
Hydrogen	SMR hydrogen	61.67	GBP/MWh
	Non-networked electrolysers	123.33	GBP/MWh
	Use of hydrogen storage	185.00	GBP/MWh
	Hydrogen load shedding	3083.33	GBP/MWh

high penalty cost for load shedding to ensure it is used only as a last resort. This high cost prioritises maintaining a reliable supply of energy, discouraging the system from choosing load shedding unless there are no other viable options, such as balancing supply and demand through other, less disruptive means. Additionally, the model assigns a relatively higher cost to electricity imports, encouraging the system to prioritise local generation and the use of domestic resources over importing electricity (this model does not consider the energy market constraints). We assume that the cost of hydrogen production from methane reformation is the cheapest, followed by non-networked hydrogen and hydrogen from storage, since flexibility of underground hydrogen storage and non-networked electrolysers is not considered in this paper.

Table 3
Scenarios definition.

Scenario No.	Flexibility resource	Limit of variation
1(baseline)	Linepack	1% variation
2		7% variation
3		13% variation
4		No limit
5	Heating	$21^\circ \pm 1^\circ$
6		$21^\circ \pm 2^\circ$
7		$21^\circ \pm 3^\circ$
8	Electrolysers	Flexible operation
9	Storage units	Flexible operation
10	All	Flexible operation (all flexible units are allowed to work within their capacity, except the heating system should maintain the indoor temperature of buildings within the range of $21^\circ \pm 3^\circ$)

4.2. Scenarios

As shown in Table 3, a total of ten scenarios have been defined to assess the effectiveness of different sources of flexibility in optimising the operation of the integrated energy system. Scenario 1 serves as the baseline representing the minimum level of flexibility. In this scenario, the heating system of the residential buildings is required to maintain the indoor temperature at 21 °C, while the electricity consumption of electrolysers, as well as electricity demand and supply by pump hydro and battery storage are not allowed to vary during the optimisation time steps. Furthermore, in the base scenario, the linepack of the hydrogen network is permitted to vary within a narrow range of 1% - large enough to avoid infeasibility due to imbalances between hydrogen supply and demand. The limit on linepack variation gradually increases to 7%, 13% and unlimited in scenarios, from 2 to 4, respectively.

To explore the value of the flexibility of the heating systems of the residential buildings, the limit on the indoor temperature range is gradually widened in Scenarios 5 to 7. Scenario 8 is designed to examine the value of flexibility offered by electrolysers, while Scenario 9 focuses on the value of flexibility offered by the storage technologies. Scenario 10 is the counterfactual to scenario 1, with all types of flexibility being available to support the operation of the integrated electricity, hydrogen and heat system. For each optimisation except for scenario 10, only one type of flexible unit is allowed. For instance, in scenarios 2-4, only linepack can be used as a source of flexibility, while the operation of all the other sources of flexibility is set to be fixed over all time steps. Additionally, all other inputs and assumptions such as hydrogen cost, ambient temperature, and wind and PV generation, are the same across all optimisations.

5. Results and discussion

This section presents and discusses the modelling results. First, the optimal operation of the integrated energy system under different scenarios is analysed to reveal how various flexibility resources influence both system performance and economic outcomes. Second, using the optimal dispatch under full-flexibility conditions as the baseline, upward and downward flexibility margins are quantified through a post-processing optimisation procedure. Finally, locational marginal prices (LMPs) are computed for different scenarios, and their relationship with nodal upward flexibility is evaluated to highlight how economic signals reflect the underlying availability of flexibility.

5.1. The value of flexibility from the energy systems integration

The electricity generation from renewable sources and non-flexible energy demands (base demand) are shown in Fig. 7a – inputs to the model. By gradually relaxing the limits for variation of linepack in the hydrogen network, as shown in Fig. 7(b1), the occurrence of hydrogen

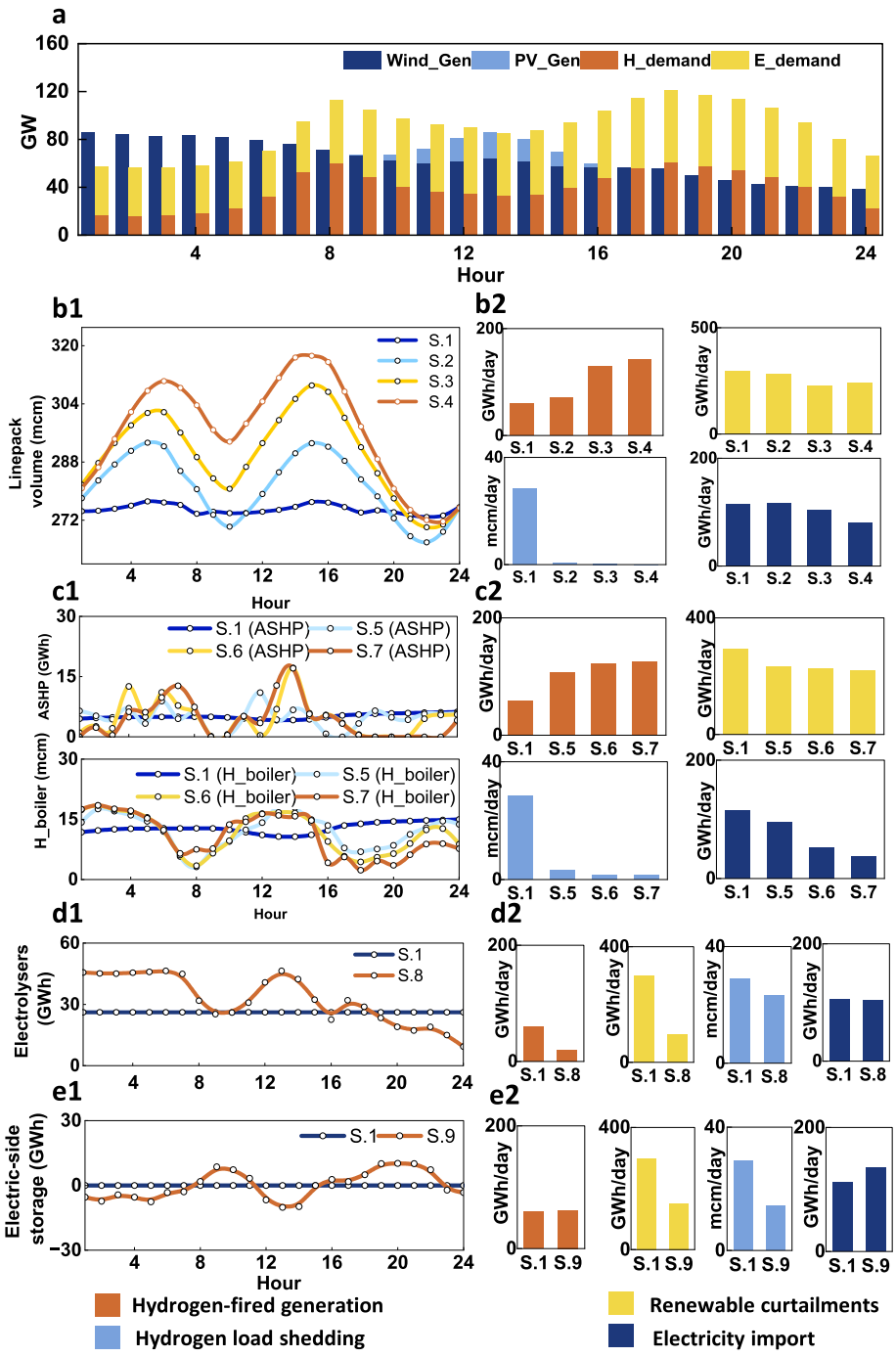

Fig. 7. Optimal operation of flexible sources in each scenario within the integrated energy. **a**, predefined[5] wind generation (Wind_Gen), PV generation (PV_Gen) and base energy demand (H_demand is base hydrogen demand and E_demand is base electricity demand). **b1**, variations of linepack under different limits. c1, variations of the energy consumption of heat pumps and hydrogen boilers. Operation of electrolysers **d1** and energy storage **e1**, with and without flexibility. **b2, c2, d2, e2** illustrate the impact of unlocking the flexibility of each type of unit on the operation of hydrogen-fired power plants, renewables curtailment, hydrogen load shedding and electricity import. S.1-S.10 in above figures correspond to Scenarios 1 through 10, respectively.

[5] The wind and PV generation profile were sourced from renewable ninja (an open-sourced platform: https://www.renewables.ninja/) and scaled according to the ratio of future generator capacity to the capacity assumed in the platform's original dataset. The baseline hydrogen and electricity demands were calculated by dividing the total estimated 2050 demand (excluding heating) by the number of days in a year.

load shedding is significantly reduced (see Fig. 7(b2)). This is due to the increased within-pipe hydrogen storage capacity of the hydrogen network to compensate for imbalances between the hydrogen supply and demand. The linepack acts as a buffer to balance the supply and the base hydrogen demand, i.e. Fig. 7(b1) indicates that linepack increases when the base hydrogen demand is low (e.g., from hour 1 to hour 6 as shown in Fig. 7a) as the excess hydrogen supply causes accumulation of hydrogen in the pipes, and linepack decreases when the base hydrogen demand reaches its peak (e.g., at hour 8). Consequently, hydrogen can be utilised more flexibly during the time it is needed the most, such as

when increasing hydrogen-fired generation can decrease the need for more expensive electricity import.

Fig. 7c demonstrates the benefits of flexibility in the residential heat sector. As illustrated by as shown in Fig. 7(c1), when indoor temperatures are allowed to vary within a range, representing the comfort temperature, electricity and hydrogen consumption by heat pumps and hydrogen boilers can be adjusted to avoid energy usage during peak periods. The flexible operation of heat pumps is mainly influenced by the gap between renewable generation and the base electricity demand, while that of hydrogen boilers is primarily affected by the profile of base hydrogen demand. By operating them flexibly, the occurrence of hydrogen load shedding and electricity import is greatly reduced, with a slight decrease in renewable curtailment, as shown in Fig. 7(c2).

Fig. 7d demonstrates that by harnessing the flexibility of electrolysers, there is a substantial reduction in the renewable energy curtailment and costly hydrogen-fired generation, since the flexible electrolysers are more capable of leveraging the renewable generation, compared to the case that those units are only allowed to working consistently. Additionally, the hydrogen load shedding is high when the flexibility of electrolysers is minimised since the restricted variation hampers electrolysers' ability to provide a steady hydrogen supply. However, with adjustable electrolysers, more hydrogen could be offered by them and thereby reducing hydrogen load shedding.

As depicted in Fig. 7e, when energy storage units are allowed to operate flexibly, they cause reductions in both renewable curtailment and hydrogen load shedding. Yet, to minimise hydrogen load shedding, there is a slight uptick in electricity imports and hydrogen-fired generation. This is because the electric-side storage units can swiftly adjust their operations, facilitating a more dynamic interaction with the grid or alternative power sources for hydrogen production or consumption, thus imparting flexibility to the hydrogen network.

Fig. 8a highlights the operational range of flexibility sources in both scenario 1 (with minimal available flexibility) and scenario 10 (where all flexibility sources are accessible). Electrolysers appear to offer greater system flexibility than electric-side storage units and heat pumps, attributed to their higher capacity. Furthermore, hydrogen boiler energy consumption can vary between 10 GWh and 60 GWh while the linepack volume can range from 825 GWh to 880 GWh, suggesting they have the potential to offer ample system flexibility.

Fig. 8b reveals that upon activating the flexibility of these flexibility resources, the integrated energy system becomes capable of accommodating significantly higher levels of renewable energy generation. This results in a reduction of approximately 70% in renewable curtailment, thereby reducing the need for electricity from interconnectors and hydrogen-fired power plants. Additionally, the requirement for hydrogen load shedding is also significantly reduced. The breakdown of the operating costs for both hydrogen and electricity are presented in Fig. 8c. It is evident that in the absence of a sufficient level of flexibility, the overall cost is substantially higher. This is primarily attributed to the expensive nature of hydrogen load shedding and electricity import.

Compared with previous studies that examine flexibility from individual sources in isolation, such as linepack flexibility [43,44] and building thermal flexibility enabled by heat pumps [45,46], the present work integrates these resources within a unified operational framework. This allows us to capture the combined and interacting value of flexibility within an integrated energy system. Looking forward, extending this unified modelling framework to encompass additional sectors such as transport and industry [17,18,20,47] could further unlock cross-sector synergies and reveal optimal interactions among heterogeneous flexibility resources, thereby providing even larger system-wide flexibility potential.

5.2. Quantifying the magnitude of flexibility available in an integrated energy system

The optimisation of the integrated energy system considering all types of flexibilities (scenario10) determines the optimal operation of flexibility resources to minimise the total operating costs. This optimisation assumes day-ahead perfect foresight, leading to the optimal use of flexibilities to compensate for variations of energy demands and supplies.

To quantify the magnitude of flexibility available at each time step to address unexpected changes in energy demands and supplies, we propose a method to elucidate the operational margin of the integrated energy system. By focusing on maximising flexibility rather than minimising costs, the maximum level of flexibility that can be provided at each time step can be quantified, subject to the constraints governing the operation of the technologies and the interdependent energy vectors. In order to calculate the maximum level of flexibility for a specific hour, certain variables (include renewable curtailments, electricity import, hydrogen-fired generation and load shedding for both hydrogen, heating and electricity) must be fixed for all time steps, since those variables are changeable and could affect quantifying the system flexibility if they are not fixed.

Some other variables associate with the basic operational constraints of the system such as pressure value of the hydrogen transmission system, pipe flow, electricity flow cannot be fixed, since they have to be adjustable to help different units providing flexibility. Additionally, the operation of each flexibility resource needs to be fixed for all time steps before the hour being optimised. This ensures that the optimisation process focuses solely on determining the flexibility provision of the flexibility resources during the target hour while keeping other variables and resource operations constant throughout the previous time steps.

We quantified the flexibility for the entire system under scenario 10 and visualised it spatiotemporally in each region as Fig. 9a shows. The distribution of locational flexibility reveals that each Busbar is distinct in terms of type and magnitude of flexibility. For instance, certain Busbars like London and those in the Midlands tend to offer downward flexibility due to relatively higher demand in those areas. On the other hand, Busbars in Scotland, characterised by higher renewables generation, find it easier to provide upward flexibility, mainly by decreasing the workload of the electrolysers.

Fig. 9b is the profile of the optimal operation of each flexibility resource in scenario 10 while Fig. 9c and d shows the share of flexibility from each flexible unit in the mix. Fig. 9c reveals that electrolysers play a predominant role in offering upward flexibility since hydrogen storage in the linepack can be used to meet the hydrogen demand. In contrast, heat pumps only provide limited upward flexibility (i.e. reducing their electricity consumption), since their energy consumption was optimised to reach the minimum operational cost of the system.

However, the manner in which each flexibility resource provides downward flexibility differs from their provision of upward flexibility [44,48]. Fig. 9d further illustrates and quantifies this behaviour, showing how different resources transition into downward flexibility provision under varying demand and renewable availability conditions. During the initial hours, it is challenging for all flexibility resources to offer downward flexibility. This can be attributed to the higher renewable generation and lower electricity demand during this period (see Fig. 7a) which caused the electrolysers and ASHP to already maximise their consumption in the day ahead schedule (i.e. Scenario 10). The total downward flexibility gradually increases from hour 1 to hour 11, as renewable generation decreases, and electricity demand rises. However, at hour 12, the total downward flexibility experiences a slight decrease due to the peak in renewable generation, particularly from solar sources. Subsequently, from hour 13 onwards, the downward flexibility mix provided by all flexibility resources begins to rise again, as their operation in the optimal profile remains far below their upper operational limit. This figure specifically shows flexibility directly offered to the electricity system through adjusting electricity demand and supply, therefore, other flexibility resources such as linepack and hydrogen boilers are not included in the quantification analysis of system flexibility magnitude.

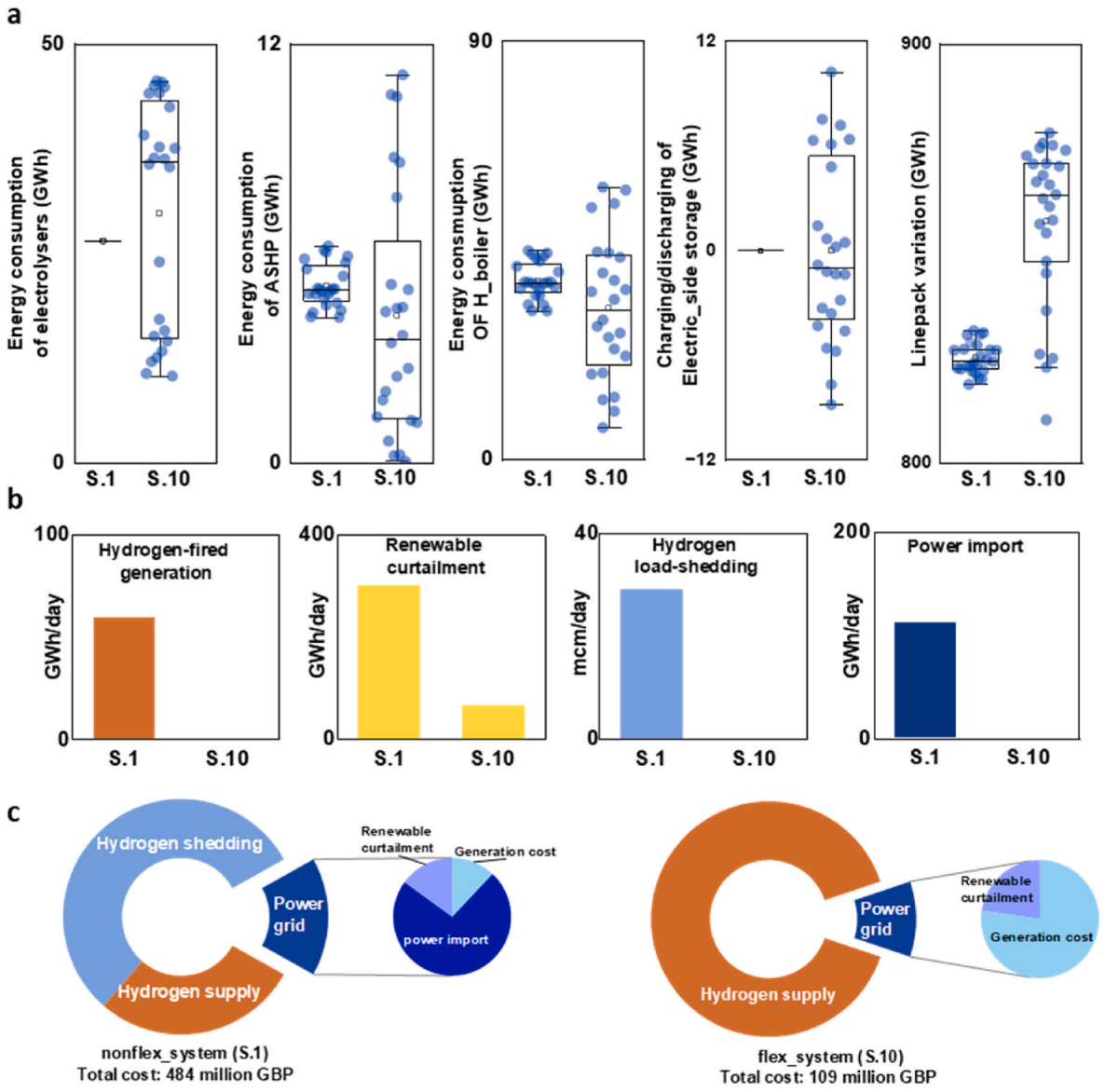

Fig. 8. Impacts of flexibility on operation of the integrated energy system. a, variations of different flexibility resources with/without flexibility. b, the impact of unlocking the flexibility of each type of unit on the operation of hydrogen-fired power plants, renewables curtailment, hydrogen load shedding and electricity import. c, the operational cost of the energy systems integration with/without flexibility.

In contrast to Section 5.1 and many existing studies that focus [45, 49,50] on the operational coordination of flexibility resources, the analysis in Section 5.2 characterises the system-level upward and downward flexibility margins under optimal dispatch. Although this is performed as a post-analysis of the optimal schedule, it still provides a direct quantitative indicator of the system's ability to accommodate external variations such as renewable generation or demand fluctuations. Because the optimisation framework is formulated as a mixed-integer non-linear problem, incorporating stochastic uncertainties would significantly increase computational burden and compromise tractability [51], therefore, uncertainties are not included in the current model.

5.3. Correlations between locational marginal price and magnitude of available flexibility

The Locational Marginal Price (LMP) serves as a pivotal indicator, effectively capturing the intrinsic value of electric energy at diverse geographical locations. It accounts for the intricate interplay between load patterns, electricity generation sources, and the physical limitations embedded within the transmission system. By considering these crucial factors, LMP offers a reflection of the economic valuation of electricity across various nodes within the grid.

While LMP values are not equivalent to the end-user electricity prices under the current GB single pricing regime, they offer valuable insights into the spatial marginal cost of electricity supply, incorporating generation costs, network congestion, and system constraints. Moreover,

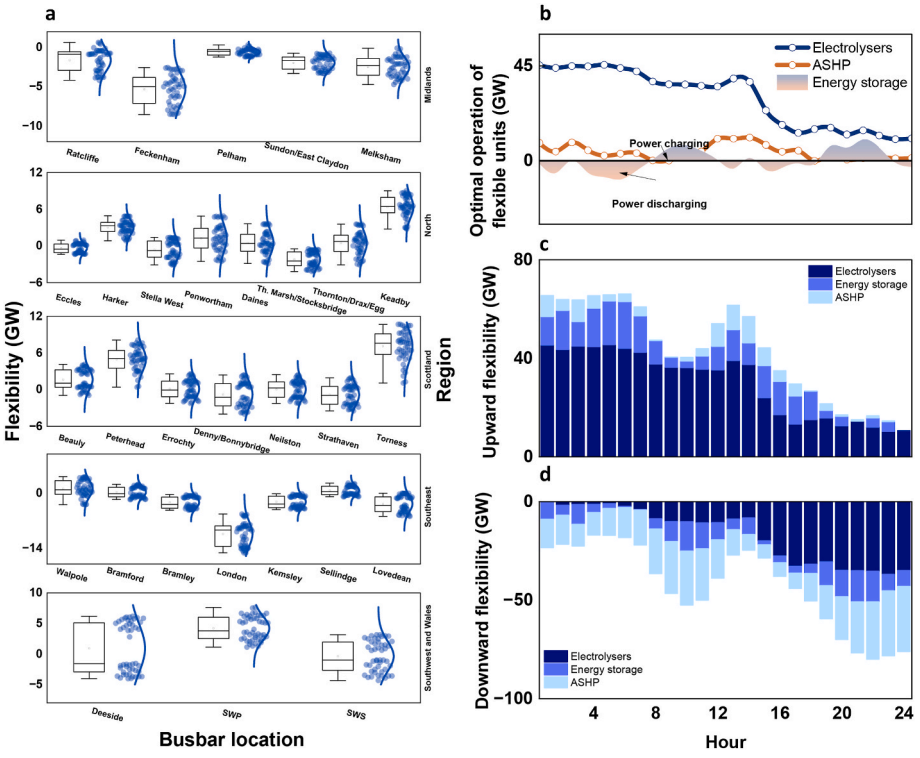

Fig. 9. **a**, Flexibility offered by each Busbar in different regions. **b**, the optimal operation of electrolysers, ASHP and power storages. **c**, the upward flexibility mix of the system, upward flexibility refers to the system's capacity to augment energy supply or reduce energy demand. **d**, the downward flexibility mix of the system, downward flexibility refers to the system's capacity to reduce energy supply while increase energy demand.

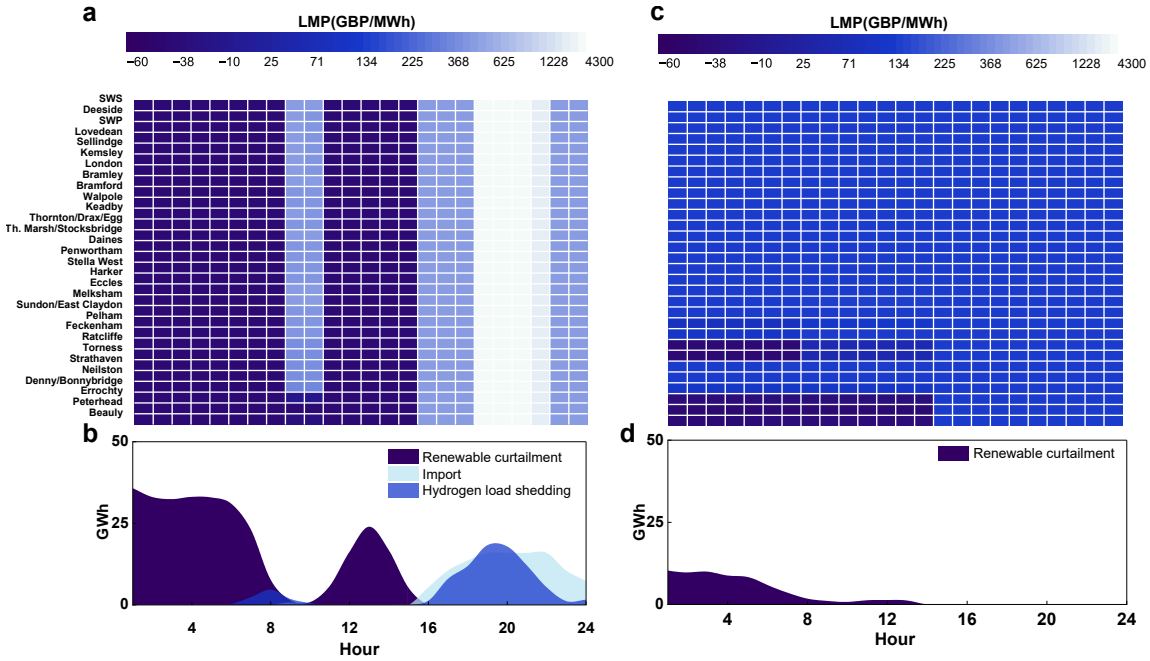

Fig. 10. Impacts of system's flexibility on LMP in the electric power system. a, LMP of the non-flexible electric power system in scenario 1. b, renewable curtailment, electricity import and hydrogen load shedding over 24 h in scenario 1. c, LMP of the flexible electric power system in scenario 10. d, renewable curtailment over 24 h in scenario 10 (no hydrogen load shedding and electricity import in this scenario).

there are ongoing policy discussions around the introduction of locational pricing in Great Britain, which could lead to LMP values directly influencing consumer prices [52]—such as in agile tariffs [53] already used by some suppliers. In this study, LMP is primarily used as an economic signal to evaluate how flexibility can alleviate network constraints and where flexibility resources would be most effective in reducing system costs.

In our study, we conducted an analysis to investigate the relationship between available local flexibility and LMP. To capture the LMP for scenarios with sufficient flexibility (scenario 10) and without such (scenario 1), we employed a dual-prime optimisation approach. The results, presented in Fig. 10, illustrate the LMP values for the electric power system under both scenarios. To elucidate the distribution of LMP values at each time step, we present the results for renewable curtailment, electricity import, and hydrogen load shedding (Fig. 10b and d). These results demonstrate the economic value of flexibility for the electric power system. From Fig. 10a, it is evident that the LMP value for the inflexible system peaks significantly during hours 19-22. This surge can largely be attributed to hydrogen load shedding and electricity imports. Conversely, during hours 1-8 and 10-16, the LMP value dips into the negatives, due to a consequence of substantial renewable curtailment. In comparison, as depicted in Fig. 10c, the system with ample flexibility exhibits a much-reduced LMP during hours 19-22. Moreover, due to the diminished renewable curtailment, only a handful of Busbars have negative LMP values at specific intervals.

Given that the LMP is a notable indicator reflecting the influence of the increase in electricity demand on the overall cost of the system, and the electric power system's upward flexibility showcases its capacity to maximise the supply minus demand, it is reasonable to expect a relationship between LMP and such flexibility [54,55]. To examine the interplay between these two factors, we use 30 profiles showing correlations between them at each Busbar over all timesteps in Fig. 11. By fitting linear curves, we visually illustrate the correlations between LMP and upward flexibility. Our analysis demonstrates a prevailing negative correlation across the majority of the plots, signifying that an increase in the system's capability to provide upward flexibility corresponds to a decrease in LMP. Note that, this relationship should not be interpreted as causality but rather as two economic manifestations of the same underlying system tightness. These findings imply that the explicit link between local flexibility potential and LMP could serve as a robust locational signal, supporting future integration of spatial pricing signals into national electricity market frameworks [56].

6. Conclusion and future work

6.1. Conclusion

As the penetration of variable renewable generation continues to increase while the capacity of unabated fossil-fuelled power stations is required to be reduced, the need for alternative sources of flexibility to support the operation of the electric power system becomes increasingly crucial. In this study, we aim to quantify the flexibility available through energy systems integration, and investigate the value of flexibility in supporting cost-effective operation of integrated energy systems.

In this study, we propose a method to quantify the magnitude and value of flexibility from energy systems integration, considering the complex interactions and interdependencies between different energy vectors and the electricity system. The presence of flexibility enables the system to optimise its operation, balancing the supply and demand of energy more efficiently, and thereby reducing costs.

Additionally, our analysis of the relation between locational marginal price of electricity and flexibility demonstrates that the availability of flexibility in a region leads to less variability in the locational marginal prices. This is attributed to the system's ability to adjust electricity demand and supply to effectively integrate and utilise renewable generation, reducing the need for curtailment, electricity import, and hydrogen load shedding which affect the marginal cost of meeting demand at different locations. The analysis reveals that in scenarios where the system lacks the capacity to accommodate high levels of renewable generation, the LMP is very sensitive to the demand and renewable generation profiles, i.e. predominantly negative during periods of high renewable generation, and significantly high during low generation and high demand periods.

Our correlation analysis between locational marginal price (LMP) and flexibility reveals that there exists an inverse relationship between the available local upward flexibility and LMP. This means that by harnessing the potential of flexibility, the system can better manage the increasing demand, through optimally dispatching renewables over timesteps.

Overall, this paper contributes to the understanding of the magnitude and value of flexibility in integrated energy systems. The findings emphasise the importance of unlocking alternative sources of flexibility in optimising system operation, reducing costs, and enhancing renewable energy integration. Additionally, the paper provides a tool for quantifying and optimising flexibility potential at different time steps. The analysis of spatial flexibility distribution and its correlation with LMP further enriches our understanding of the economic implications of flexibility.

6.2. Future work

In this paper, an effective model framework for the integrated energy system (IES) was developed. This framework is applicable to a variety of cases and scenarios, enabling the exploration of complex interactions between different sectors within the energy system. However, the complexity of the mathematical model, which includes a large number of binary variables and nonlinear constraints to represent the operational status of certain facilities and hydraulic flow within various pipelines, limits its application for long-term optimisation. As a result, the current analysis focuses on short-term system operation and does not explicitly capture seasonal variations in energy demand, ambient temperature, and renewable resource availability. These seasonal characteristics play a critical role in shaping system operating conditions and are essential for a comprehensive assessment of flexibility in integrated energy systems. Future work will therefore consider representative operating periods across different seasons and, where appropriate, incorporate uncertainty in key drivers such as renewable generation and temperature to further examine the robustness of system flexibility under a wider range of operating conditions.

In addition, while this work focuses on the operational interactions among electricity, hydrogen, and residential heating systems, emerging flexibility resources from transport and industrial electrification—such as smart EV charging, vehicle-to-grid services, and industrial thermal energy storage—represent promising extensions of the modelling scope for future research, and would allow further assessment of cross-sector flexibility synergies within a unified modelling framework.

Future improvements could also involve integrating advanced techniques, such as physics-informed data-driven methods, to enhance the model's computational performance and scalability. This would facilitate long-term planning analyses that explicitly account for uncertainty. Such enhancements would allow the model to offer deeper insights, including the seasonal provision of both heating and cooling

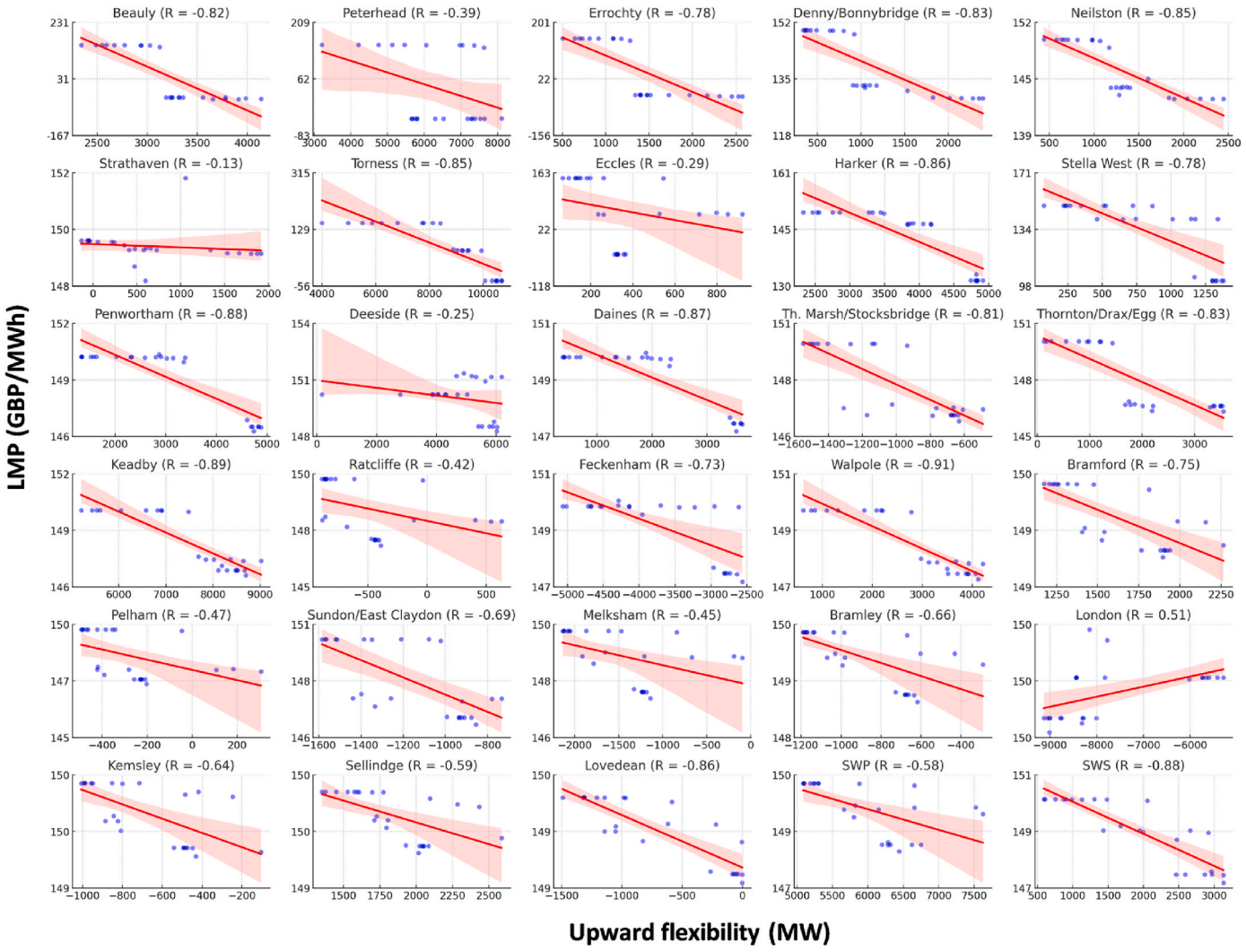

Fig. 11. Matrix of correlations between LMP and upward flexibility at each Busbar. Blue bubbles represents the relationship between flexibility (x-axis) and LMP (y-axis) across all timesteps at each Busbar. The linear fitting curve illustrates the correlation between these variables. A smaller R-value indicates a stronger negative correlation between LMP and upward flexibility.

flexibility from the building sector, the identification of more efficient pathways toward Net Zero, and more informed investment decisions regarding the deployment of low-carbon technologies.

CRediT authorship contribution statement

Qikun Chen: Writing – review & editing, Writing – original draft, Visualization, Validation, Software, Methodology, Investigation, Formal analysis, Data curation, Conceptualization. **Meysam Qadrdan:** Writing – review & editing, Supervision, Project administration, Methodology, Funding acquisition, Conceptualization.

Declaration of competing interest

The authors declare no competing interests.

Acknowledgement

This work was supported by the UK Research and Innovation (UKRI) via Hydrogen Integration for Accelerated Energy Transitions Hub (EP/X038823/2).

Appendix 1. Simplified GB energy systems

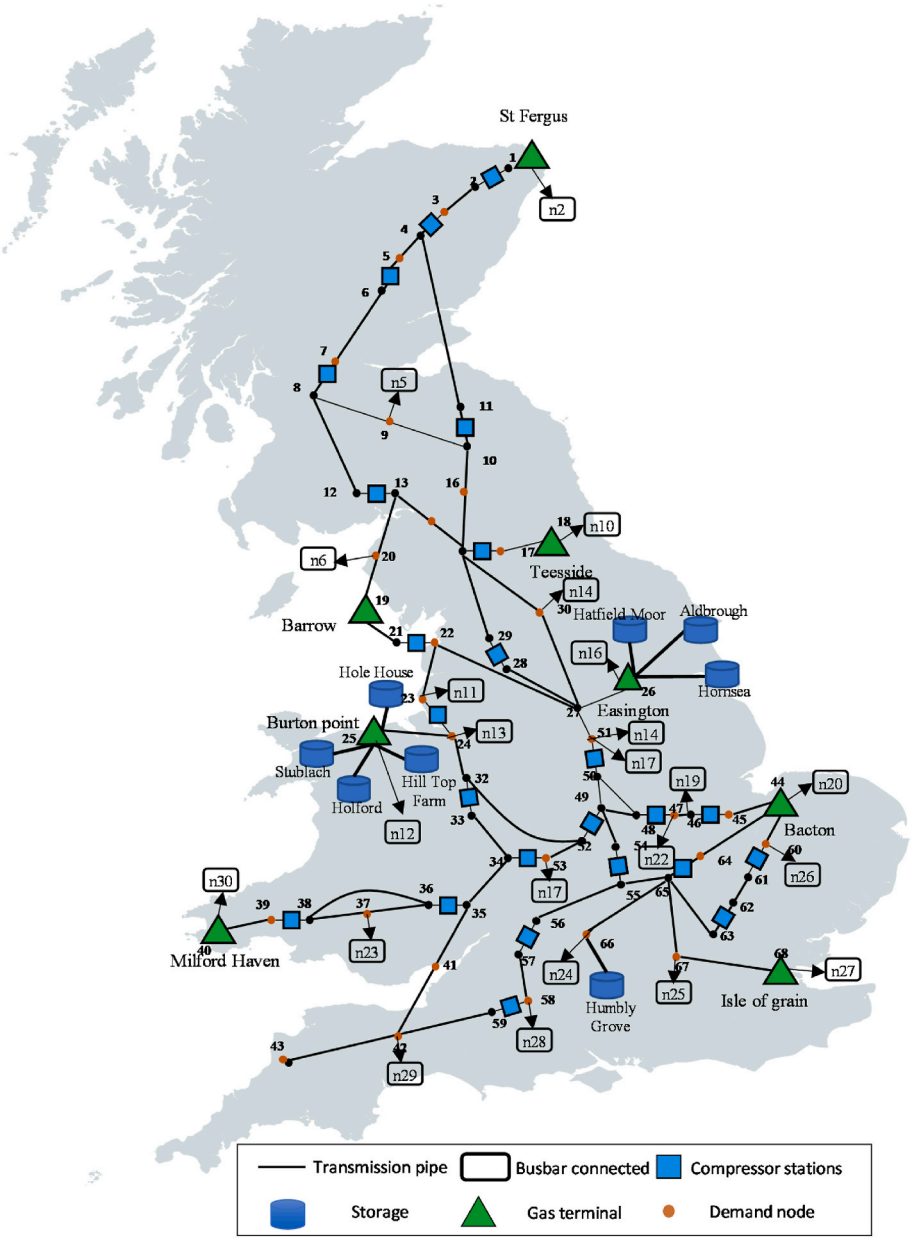

Fig. a. A simplified hydrogen transmission system.

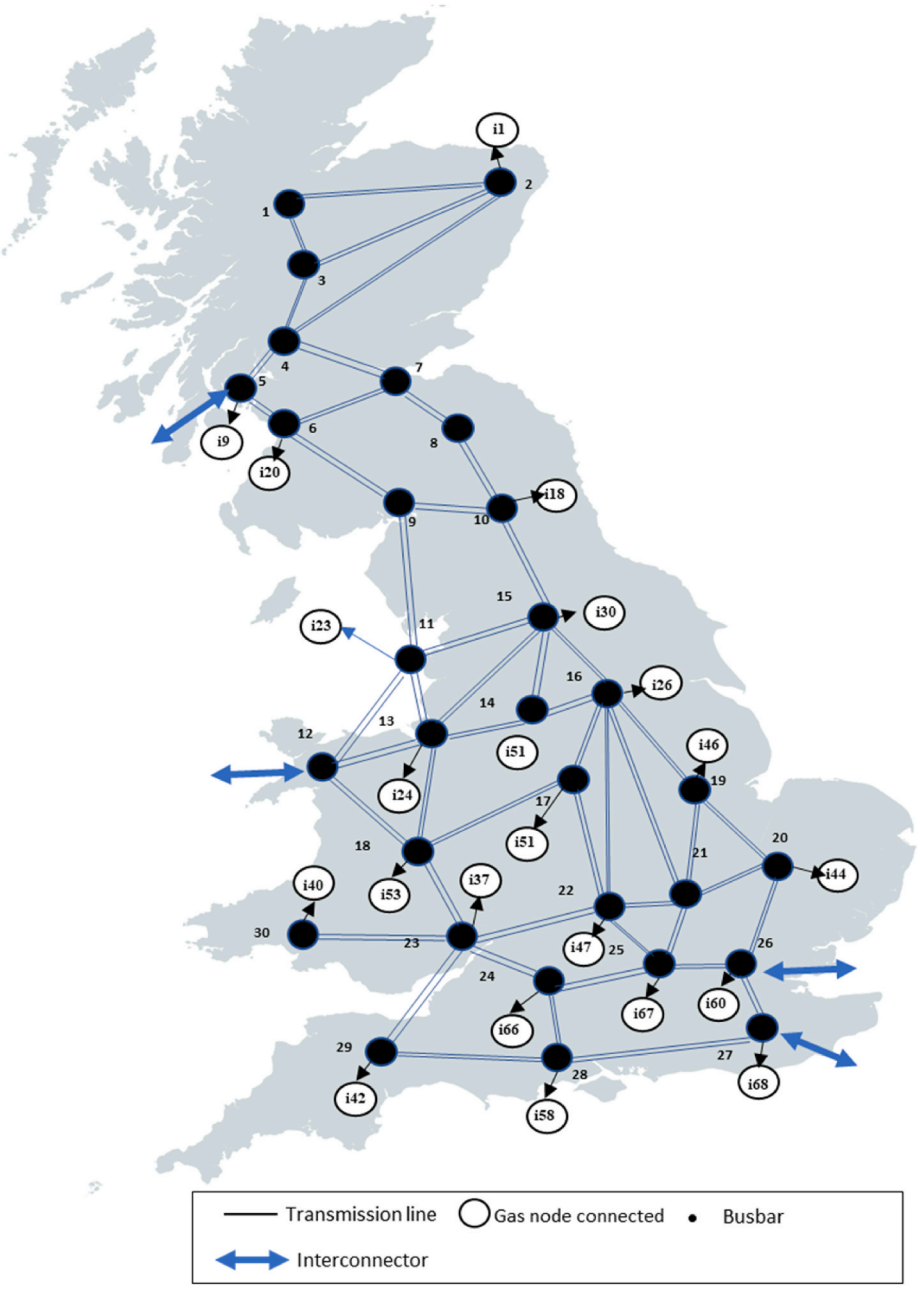

Fig. b. A simplified electricity transmission system.

Appendix 2

A2.1 Reformulation of the Mixed-Integer Nonlinear Problem

Due to the nonlinear and nonconvex nature of Eq. (6), which characterises the intricate bidirectional flow within the pipeline, solving it presents a substantial computational challenge for optimisations. To overcome this obstacle, we introduce an efficient approximation approach to tackle the problem. To formulate the bidirectional flow, a set of auxiliary variables are introduced, as Eq. (A1) and Eq. (A2) denoted. Then Eq. (5) can be replaced by Eq. (A3).

$$Q^{+}_{p,t} = 0.5\left(Q^{\text{in}+}_{p,t} + Q^{\text{out}+}_{p,t}\right), \forall p \in P, \forall t \in T \tag{A1}$$

$$Q^{-}_{p,t} = 0.5\left(Q^{\text{in}-}_{p,t} + Q^{\text{out}-}_{p,t}\right), \forall p \in P, \forall t \in T \tag{A2}$$

$$Q^{\text{AV}}_{p,t} = Q^{+}_{p,t} - Q^{-}_{p,t}, \forall p \in P, \forall t \in T \tag{A3}$$

Then, a sufficiently large value M^F are employed, with a set of binary variables $x_{p,t}$ in Eq. (A4) and Eq. (A5), to ensure either $Q^+_{p,t}$ or $Q^-_{p,t}$ is active, that is, when $x_{p,t} = 1$, $Q^+_{p,t}$ is active and $Q^-_{p,t} = 0$, otherwise, $Q^-_{p,t}$ is active and $Q^+_{p,t} = 0$. Then, Eq. (6) can be replaced by Eq. (A6) – Eq. (A9).

$$0 \le Q^+_{p,t} \le M^F x_{p,t}, \forall p \in P, \forall t \in T \tag{A4}$$

$$0 \le Q^-_{p,t} \le M^F (1 - x_{p,t}), \forall p \in P, \forall t \in T \tag{A5}$$

$$\left(Q^+_{p,t}\right)^2 \le K^2_{p,t}\left(\Pi^2_{n^{start},t} - \Pi^2_{n^{end},t}\right) + \left(M^F\right)^2 (1 - x_{p,t}), \forall p \in P, \forall t \in T \tag{A6}$$

$$\left(Q^+_{p,t}\right)^2 \ge K^2_{p,t}\left(\Pi^2_{n^{start},t} - \Pi^2_{n^{end},t}\right) - \left(M^F\right)^2 (1 - x_{p,t}), \forall p \in P, \forall t \in T \tag{A7}$$

$$\left(Q^-_{p,t}\right)^2 \le -K^2_{p,t}\left(\Pi^2_{n^{start},t} - \Pi^2_{n^{end},t}\right) + \left(M^F\right)^2 (x_{p,t}), \forall p \in P, \forall t \in T \tag{A8}$$

$$\left(Q^-_{p,t}\right)^2 \ge -K^2_{p,t}\left(\Pi^2_{n^{start},t} - \Pi^2_{n^{end},t}\right) - \left(M^F\right)^2 (x_{p,t}), \forall p \in P, \forall t \in T \tag{A9}$$

Next, the Polyhedral Outer-Approximation (POA) is employed, to relax the quadratic term $\left(Q^+_{p,t}\right)^2$, $\left(Q^-_{p,t}\right)^2$. This method revolves around the approximation of a non-linear feasible region using a polyhedral set. Outer tangent lines are constructed at select points along the curve of the non-linear function, establishing its lower bounds. Concurrently, a straight line connecting both ends of this curve is employed to define the upper bound. Fig. A1 provides a graphical representation of an example using this approximation technique on a quadratic function $f(Q) = Q^2$.

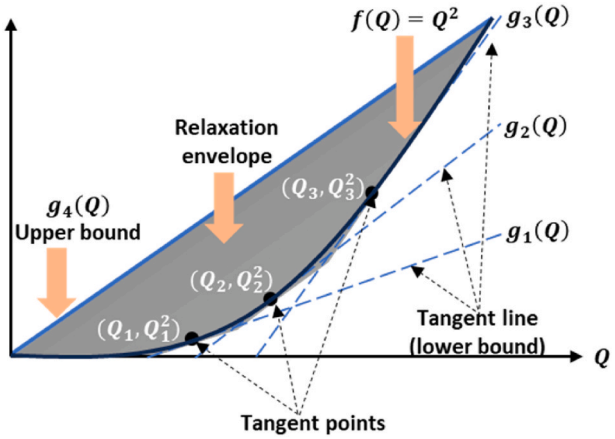

Fig. A1. Approximating a quadratic function using POA.

Firstly, choosing three points along the curve (Q_1, Q_1^2), (Q_2, Q_2^2), (Q_3, Q_3^2), and then creating outer tangents at these points as described by Eq. (A10). These tangent lines serve as the lower boundary of $f(Q)$, as expressed by Eq. (A11). The upper bound of $f(Q)$ can be denoted by Eq. (A12) where $(Q_s, f(Q_e))$, $(Q_e, f(Q_s))$, represent both ends of the curve. Then, Eq. (A6) – Eq. (A9) can be reformulated to Eq. (A13) – Eq. (A16).

$$\varphi_i(Q) - f(Q_i) = \frac{df(Q_i)}{dQ_i}(Q - Q_i), i = 1, 2, 3 \tag{A10}$$

$$f(Q) \ge \varphi_i(Q), i = 1, 2, 3 \tag{A11}$$

$$f(Q) \le \frac{f(Q_e) - f(Q_s)}{Q_e - Q_s}(Q - x_e) + f(Q_e) \tag{A12}$$

$$\varphi_i\left(Q^+_{p,t}\right) \le K^2_{p,t}\left(\Pi^2_{n^{start},t} - \Pi^2_{n^{end},t}\right) + \left(M^F\right)^2 (1 - x_{p,t}), \forall p \in P, \forall t \in T \tag{A13}$$

$$\varphi_i\left(Q^+_{p,t}\right) \ge K^2_{p,t}\left(\Pi^2_{n^{start},t} - \Pi^2_{n^{end},t}\right) - \left(M^F\right)^2 (1 - x_{p,t}), \forall p \in P, \forall t \in T \tag{A14}$$

$$\varphi_i\left(Q^-_{p,t}\right) \le -K^2_{p,t}\left(\Pi^2_{n^{start},t} - \Pi^2_{n^{end},t}\right) + \left(M^F\right)^2 (x_{p,t}), \forall p \in P, \forall t \in T \tag{A15}$$

$$\varphi_i\left(Q^-_{p,t}\right) \ge -K^2_{p,t}\left(\Pi^2_{n^{start},t} - \Pi^2_{n^{end},t}\right) - \left(M^F\right)^2 (x_{p,t}), \forall p \in P, \forall t \in T \tag{A16}$$

Now, introducing $\psi^-_{p,t} = \Pi_{n^{start},t} - \Pi_{n^{end},t}$ and $\psi^+_{a,t} = \Pi_{n^{start},t} + \Pi_{n^{end},t}$, then the nonlinear term $\Pi^2_{n^{start},t} - \Pi^2_{n^{end},t}$ can be converted to a linear term by using $\varphi_{p,t} = \psi^-_{p,t}\psi^+_{p,t}$. Then McCormick envelope is employed to relax the bilinear term as shown in Fig. A2. The four lines used to enclose the relaxation envelope is expressed by Eq. (A17) – Eq. (A20).

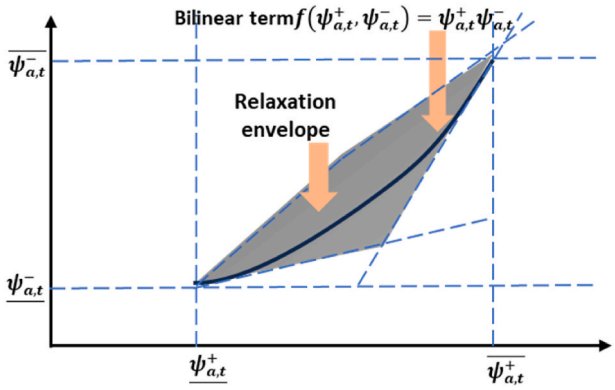

Fig. A2. Relaxing bilinear term using MCcormick envelope.

$$\varphi_{p,t} \geq \psi^-_{p,t}\overline{\psi^+_{p,t}} + \overline{\psi^-_{p,t}}\psi^+_{p,t} - \overline{\psi^-_{p,t}}\,\overline{\psi^+_{p,t}}, \forall p \in P, \forall t \in T \tag{A17}$$

$$\varphi_{p,t} \geq \psi^-_{p,t}\underline{\psi^+_{p,t}} + \underline{\psi^-_{p,t}}\psi^+_{p,t} - \underline{\psi^-_{p,t}}\,\underline{\psi^+_{p,t}}, \forall p \in P, \forall t \in T \tag{A18}$$

$$\varphi_{p,t} \leq \psi^-_{p,t}\overline{\psi^+_{p,t}} + \underline{\psi^-_{p,t}}\psi^+_{p,t} - \underline{\psi^-_{p,t}}\,\overline{\psi^+_{p,t}}, \forall p \in P, \forall t \in T \tag{A19}$$

$$\varphi_{p,t} \leq \psi^-_{p,t}\underline{\psi^+_{p,t}} + \overline{\psi^-_{p,t}}\psi^+_{p,t} - \overline{\psi^-_{p,t}}\,\underline{\psi^+_{p,t}}, \forall p \in P, \forall t \in T \tag{A20}$$

A2.2 Comparison of nonlinearity approximations performances

Apart from the relaxation method used in this study, other techniques—such as piecewise linear (PWL) approximation and second-order cone (SOC) relaxation—are also commonly applied to approximate nonlinear gas flow equations. While PWL offers higher accuracy, it often results in long computation times and convergence issues in large-scale systems (e.g., failure to converge within 10 h in our case study). SOC relaxation is computationally more efficient but tends to produce overly relaxed solutions that compromise accuracy. To balance accuracy and tractability, we adopt McCormick relaxation combined with outer approximation, which proves faster than PWL and more accurate than SOC. In our tests, computation times ranged from 5 min to 2 h depending on the scenario, using a MacBook Air with an M3 chip and 16 GB of RAM. A small-scale validation case further confirms that this method maintains acceptable accuracy—typically within 30% error—while offering good computational performance, as illustrated in Fig. A3.

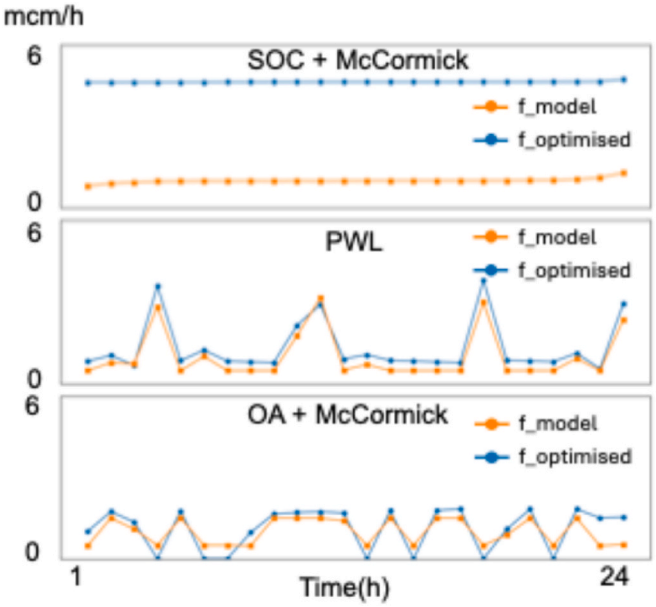

Fig. A3. Comparison of modelled and optimised gas flows under three reformulation techniques: SOC + McCormick, Piecewise Linear (PWL), and OA + McCormick.

A2.3 Sensitivity Analysis of LMPs: Fixed-Integer vs Relaxed Binary Case

To verify the robustness of the Locational Marginal Prices (LMPs) with respect to the integer decisions in the optimisation model, a comparative sensitivity analysis was performed. In the original configuration, the full Mixed-Integer Problem (MIP) was solved and the LMPs were obtained by

fixing all binary variables at their optimal integer values and calculating the dual variables of the nodal power balance constraints of the resulting LP. To evaluate the influence of binary variables, a relaxed case was constructed in which only the unit-commitment binary variables were relaxed to continuous variables in [0,1], while the gas-flow direction binaries were retained and fixed to preserve the physical feasibility of the hydrogen network. LMPs were recalculated for this relaxed case and compared against those from the fixed-binary case. The observed deviations in LMPs across all buses and time periods were small (0.3%–4%), demonstrating that the reported price signals are stable and supporting the validity of the conclusions drawn in the main text. We visualise the LMPs for both cases using heatmaps in Fig. A4(a) and A4(b), and we further present the element-wise disparities between the two sets of LMPs in Fig. A4(c).

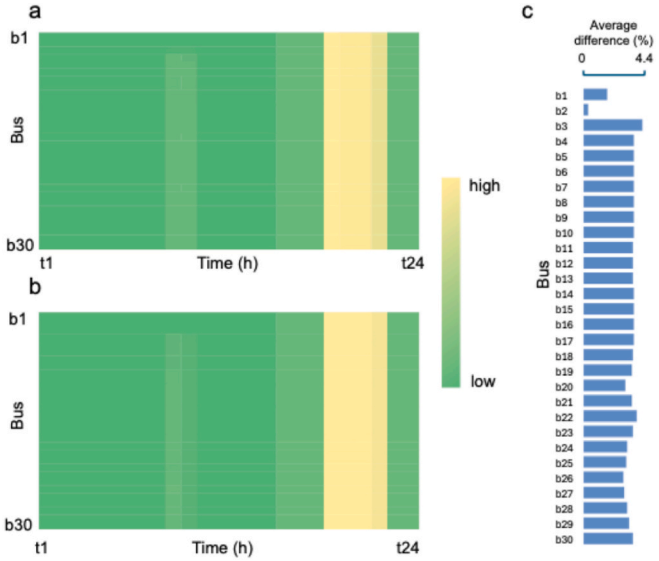

Fig. A4. Sensitivity of LMPs to binary relaxation. (a) LMP heatmap obtained from the fixed-binary case, where all binary variables are fixed at their optimal integer values. (b) LMP heatmap obtained from the relaxed-binary case, where unit-commitment binaries are relaxed to continuous values while gas flow direction binaries remain fixed. (c) Average percentage difference in LMPs over the 24-h horizon for each bus.

Data availability

Representative input datasets used in the modelling framework, including network topology, generation capacities and renewable energy profiles, are available at Zenodo: https://doi.org/10.5281/zenodo.18664748.

References

[1] LCP. Renewable curtailment and the role of long duration storage. 2022.
[2] Ofgem. Transitioning to a net zero energy system. Smart systems and flexibility plan 2021. 2021.
[3] National grid. Future energy scenarios. 2022.
[4] Hunter CA, Penev MM, Reznicek EP, Eichman J, Rustagi N, Baldwin SF. Techno-economic analysis of long-duration energy storage and flexible power generation technologies to support high-variable renewable energy grids. Joule 2021;5:2077–101. https://doi.org/10.1016/j.joule.2021.06.018.
[5] Guerra OJ, Eichman J, Kurtz J, Hodge B-M. Cost competitiveness of electrolytic hydrogen. Joule 2019;3:2425–43. https://doi.org/10.1016/j.joule.2019.07.006.
[6] Sepulveda NA, Jenkins JD, Edington A, Mallapragada DS, Lester RK. The design space for long-duration energy storage in decarbonized power systems. Nat Energy 2021;6:506–16. https://doi.org/10.1038/s41560-021-00796-8.
[7] Glenk G, Reichelstein S. Economics of converting renewable power to hydrogen. Nat Energy 2019;4:216–22. https://doi.org/10.1038/s41560-019-0326-1.
[8] Peng P, Anastasopoulou A, Brooks K, Furukawa H, Bowden ME, Long JR, et al. Cost and potential of metal–organic frameworks for hydrogen back-up power supply. Nat Energy 2022;7:448–58. https://doi.org/10.1038/s41560-022-01013-w.
[9] Huang J, Xie Y, Yan L, Wang B, Kong T, Dong X, et al. Decoupled amphoteric water electrolysis and its integration with Mn–Zn battery for flexible utilization of renewables. Energy Environ Sci 2021;14:883–9. https://doi.org/10.1039/D0EE03639K.
[10] Department for Energy Security & Net Zero. Capacity market: consumer-led flexibility. https://www.gov.uk/government/calls-for-evidence/capacity-market-consumer-led-flexibility/capacity-market-consumer-led-flexibility-html#:~:text=The%20National%20Energy%20System%20Operator,to%20ensure%20security%20of%20supply. [Accessed 6 April 2025].
[11] Canet A, Qadrdan M. Quantification of flexibility from the thermal mass of residential buildings in England and Wales. Appl Energy 2023;349:121616. https://doi.org/10.1016/j.apenergy.2023.121616.
[12] Qin H, Yu Z, Li T, Liu X, Li L. Energy-efficient heating control for nearly zero energy residential buildings with deep reinforcement learning. Energy 2023;264:126209. https://doi.org/10.1016/j.energy.2022.126209.
[13] Zhang Y, Johansson P, Sasic Kalagasidis A. Feasibilities of utilizing thermal inertia of district heating networks to improve system flexibility. Appl Therm Eng 2022;213:118813. https://doi.org/10.1016/j.applthermaleng.2022.118813.
[14] Jansen J, Jorissen F, Helsen L. Optimal control of a fourth generation district heating network using an integrated non-linear model predictive controller. Appl Therm Eng 2023;223:120030. https://doi.org/10.1016/j.applthermaleng.2023.120030.
[15] Hot water association. Hot water cylinders. n.d. https://www.hotwater.org.uk/connected-hot-water-cylinders/#:~:text=The%20Thermal%20solution,customers%20for%20that%20excess%20capacity. [Accessed 8 December 2025].
[16] Salpakari J, Mikkola J, Lund PD. Improved flexibility with large-scale variable renewable power in cities through optimal demand side management and power-to-heat conversion. Energy Convers Manag 2016;126:649–61. https://doi.org/10.1016/j.enconman.2016.08.041.
[17] Kirkerud JG, Bolkesjø TF, Trømborg E. Power-to-heat as a flexibility measure for integration of renewable energy. Energy 2017;128:776–84. https://doi.org/10.1016/j.energy.2017.03.153.
[18] Sagaria S, van der Kam M, Boström T. Vehicle-to-grid impact on battery degradation and estimation of V2G economic compensation. Appl Energy 2025;377:124546. https://doi.org/10.1016/j.apenergy.2024.124546.
[19] Upputuri RP, Subudhi B. A comprehensive review and performance evaluation of bidirectional charger topologies for V2G/G2V operations in EV applications. IEEE Trans Trans Elect 2024;10:583–95. https://doi.org/10.1109/TTE.2023.3289965.
[20] Lund H, Østergaard PA, Connolly D, Mathiesen BV. Smart energy and smart energy systems. Energy 2017;137:556–65. https://doi.org/10.1016/j.energy.2017.05.123.
[21] Lund H, Østergaard PA, Yuan M, Sorknæs P, Thellufsen JZ. Energy balancing and storage in climate-neutral smart energy systems. Renew Sustain Energy Rev 2025;209:115141. https://doi.org/10.1016/j.rser.2024.115141.
[22] Borasio M, Moret S. Deep decarbonisation of regional energy systems: a novel modelling approach and its application to the Italian energy transition. Renew Sustain Energy Rev 2022;153:111730. https://doi.org/10.1016/j.rser.2021.111730.
[23] Gonzalez JM, Tomlinson JE, Martínez Ceseña EA, Basheer M, Obuobie E, Padi PT, et al. Designing diversified renewable energy systems to balance multisector performance. Nat Sustain 2023;6:415–27. https://doi.org/10.1038/s41893-022-01033-0.
[24] Zeyringer M, Price J, Fais B, Li P-H, Sharp E. Designing low-carbon power systems for Great Britain in 2050 that are robust to the spatiotemporal and inter-annual

variability of weather. Nat Energy 2018;3:395–403. https://doi.org/10.1038/s41560-018-0128-x.
[25] Zantye MS, Arora A, Hasan MMF. Renewable-integrated flexible carbon capture: a synergistic path forward to clean energy future. Energy Environ Sci 2021;14:3986–4008. https://doi.org/10.1039/D0EE03946B.
[26] Pickering B, Lombardi F, Pfenninger S. Diversity of options to eliminate fossil fuels and reach carbon neutrality across the entire European energy system. Joule 2022;6:1253–76. https://doi.org/10.1016/j.joule.2022.05.009.
[27] Guo F, van Ruijven BJ, Zakeri B, Zhang S, Chen X, Liu C, et al. Implications of intercontinental renewable electricity trade for energy systems and emissions. Nat Energy 2022;7:1144–56. https://doi.org/10.1038/s41560-022-01136-0.
[28] Chen Z, Yiliang X, Hongxia Z, Yujie G, Xiongwen Z. Optimal design and performance assessment for a solar powered electricity, heating and hydrogen integrated energy system. Energy 2023;262:125453. https://doi.org/10.1016/j.energy.2022.125453.
[29] Li Z, Xia Y, Bo Y, Wei W. Optimal planning for electricity-hydrogen integrated energy system considering multiple timescale operations and representative time-period selection. Appl Energy 2024;362:122965. https://doi.org/10.1016/j.apenergy.2024.122965.
[30] Franken L, Hackett A, Lizana J, Riepin I, Jenkinson R, Lyden A, et al. Power system benefits of simultaneous domestic transport and heating demand flexibility in Great Britain's energy transition. Appl Energy 2025;377:124522. https://doi.org/10.1016/j.apenergy.2024.124522.
[31] Clegg S, Mancarella P. Integrated electrical and gas network flexibility assessment in low-carbon multi-energy systems. IEEE Trans Sustain Energy 2016;7:718–31. https://doi.org/10.1109/TSTE.2015.2497329.
[32] Langevin J, Harris CB, Satre-Meloy A, Chandra-Putra H, Speake A, Present E, et al. US building energy efficiency and flexibility as an electric grid resource. Joule 2021;5:2102–28. https://doi.org/10.1016/j.joule.2021.06.002.
[33] de Chalendar JA, Glynn PW, Benson SM. City-scale decarbonization experiments with integrated energy systems. Energy Environ Sci 2019;12:1695–707. https://doi.org/10.1039/C8EE03706J.
[34] Seward W, Qadrdan M, Jenkins N. Revenue stacking for behind the meter battery storage in energy and ancillary services markets. Elec Power Syst Res 2022;211:108292. https://doi.org/10.1016/j.epsr.2022.108292.
[35] Mimica M, Boras I-P, Krajačić G. The integration of the battery storage system and coupling of the cooling and power sector for increased flexibility under the consideration of energy and reserve market. Energy Convers Manag 2023;286:117005. https://doi.org/10.1016/j.enconman.2023.117005.
[36] CE-080 Natural Gas Pipeline Flow Calculations | PDH STAR. CE-080 natural gas pipeline flow calculations | PDH STAR. n.d.
[37] Wang D, Zhi Y, Jia H, Hou K, Zhang S, Du W, et al. Optimal scheduling strategy of district integrated heat and power system with wind power and multiple energy stations considering thermal inertia of buildings under different heating regulation modes. Appl Energy 2019;240:341–58. https://doi.org/10.1016/j.apenergy.2019.01.199.
[38] IEA. Flexibility by implementation of heat pump in multi-vector energy systems and thermal networks. 2023.
[39] National gas. Project union n.d. https://www.nationalgas.com/future-energy/hydrogen/project-union (accessed July 2, 2025)..
[40] National Grid ESO. FES 2023 data workbook. 2023.
[41] National grid ESO. Electricity ten year statement. 2022.
[42] Canet A, Qadrdan M, Jenkins N, Wu J. Spatial and temporal data to study residential heat decarbonisation pathways in England and Wales. Sci Data 2022;9:246. https://doi.org/10.1038/s41597-022-01356-9.
[43] Chen Q, Zhao Y, Qadrdan M, Jenkins N. Optimal operation of compressors in an integrated gas and electricity system—an enhanced MISOCP method. IEEE Access 2022;10:131489–97. https://doi.org/10.1109/ACCESS.2022.3227859.
[44] Chen Q, Zhang T, Qadrdan M. Assessing techno-economic and environmental impacts of gas compressor fleet as a source of flexibility to the power system. IEEE Trans Energy Mark, Policy Regul 2023;1:274–85. https://doi.org/10.1109/TEMPR.2023.3276308.
[45] Chen Q, Liu L. Revealing trade-offs between flexibility and equity in an integrated electricity-heating system. Appl Energy 2025;400:126624. https://doi.org/10.1016/j.apenergy.2025.126624.
[46] Chen Q, Qadrdan M. Flexible operation of heat pumps in a decarbonised power system. 2024 IEEE PES innovative smart grid technologies Europe (ISGT EUROPE). IEEE; 2024. p. 1–7. https://doi.org/10.1109/ISGTEUROPE62998.2024.10863519.
[47] Gabrek N, Seifermann S. How the correlation between electricity prices and emission intensity affects the economic and ecological potential of industrial demand-side flexibility measures. J Clean Prod 2025;518:145863. https://doi.org/10.1016/j.jclepro.2025.145863.
[48] Zhao Y, Xu X, Qadrdan M, Wu J. Optimal operation of compressor units in gas networks to provide flexibility to power systems. Appl Energy 2021;290:116740. https://doi.org/10.1016/j.apenergy.2021.116740.
[49] Karimi H, Jadid S. Multi-layer energy management of smart integrated-energy microgrid systems considering generation and demand-side flexibility. Appl Energy 2023;339:120984. https://doi.org/10.1016/j.apenergy.2023.120984.
[50] Rao AK, Bolorinos J, Musabandesu E, Chapin FT, Mauter MS. Valuing energy flexibility from water systems. Nat Water 2024;2:1028–37. https://doi.org/10.1038/s44221-024-00316-4.
[51] He F, Qu R. A two-stage stochastic mixed-integer program modelling and hybrid solution approach to portfolio selection problems. Inf Sci 2014;289:190–205. https://doi.org/10.1016/j.ins.2014.08.028.
[52] Simon Gill KB and CM. The potential impact of locational marginal pricing 2023. https://ukerc.ac.uk/news/potential-lmp-impacts/. [Accessed 2 July 2025].
[53] Octopus energy. Agile pricing explained. n.d. https://octopus.energy/blog/agile-pricing-explained/. [Accessed 2 July 2025].
[54] Zhao Z, Liu Y, Guo L, Bai L, Wang Z, Wang C. Distribution locational marginal pricing under uncertainty considering coordination of distribution and wholesale markets. IEEE Trans Smart Grid 2023;14:1590–606. https://doi.org/10.1109/TSG.2022.3200704.
[55] Wang H, Bie Z, Ye H. Locational marginal pricing for flexibility and uncertainty with moment information. IEEE Trans Power Syst 2023;38:2761–75. https://doi.org/10.1109/TPWRS.2022.3196155.
[56] UKERC. Locational signals for electricity system flexibility alongside a national wholesale market. https://ukerc.ac.uk/news/locational-signals-for-electricity-system-flexibility-alongside-a-national-wholesale-market/. [Accessed 9 December 2025].